AD A068915

LEVEL II

RADC-TR-79-45
Interim Report
April 1979

HIGH POWER MILLIMETER WAVE AMPLIFIER

Varian Associates, Inc.

DDC
RECEIVED
MAY 24 1979
C

Sponsored by
Defense Advanced Research Projects Agency (DoD)
ARPA Order No. 3192

Ballistic Missile Defense
Advanced Technology Center (Army)

APPROVED FOR PUBLIC RELEASE; DISTRIBUTION UNLIMITED

The views and conclusions contained in this document are those of the authors and should not be interpreted as necessarily representing the official policies, either expressed or implied, of the Defense Advanced Research Projects Agency or the U.S. Government.

ROME AIR DEVELOPMENT CENTER
Air Force Systems Command
Griffiss Air Force Base, New York 13441

79 05 21 015

This report has been reviewed by the RADC Information Office (OI) and is releasable to the National Technical Information Service (NTIS). At NTIS it will be releasable to the general public, including foreign nations.

RADC-TR-79-45 has been reviewed and is approved for publication.

APPROVED: Kevin O'Brien

KEVIN O'Brien, 1/Lt, USAF
Project Engineer

If your address has changed or if you wish to be removed from the RADC mailing list, or if the addressee is no longer employed by your organization, please notify RADC (OCTP) Griffiss AFB NY 13441. This will assist us in maintaining a current mailing list.

Do not return this copy. Retain or destroy.

HIGH POWER MILLIMETER WAVE AMPLIFIER

S. Heji
H. Jory
A. Karp
R. Morwood
A. Nordquist
R. Symons

Contractor: Varian Associates, Inc.
Contract Number: F30602-78-C-0011
Effective Date of Contract: 31 October 1977
Contract Expiration Date: 31 October 1979
Short Title of Work: High Power Millimeter Wave Amplifier
Program Code Number: 6E20
Period of Work Covered: Mar 1978 - Nov 1978

Principal Investigator: Howard Jory
Phone: 415 493-4000

Project Engineer: 1/Lt Kevin O'Brien
Phone: 315 330-4381

Approved for public release; distribution unlimited.

This research was supported by the Defense Advanced Research Projects Agency of the Department of Defense and was monitored by 1/Lt Kevin O'Brien (OCTP), Griffiss AFB NY 13441 under Contract F30602-78-C-0011.

ACCESSION for
NTIS White Section
DDC Buff Section
UNANNOUNCED
JUSTIFICATION
BY
DISTRIBUTION/AVAILABILITY CODES
Dist. AVAIL. and/or SPECIAL
A

UNCLASSIFIED

SECURITY CLASSIFICATION OF THIS PAGE (When Data Entered)

REPORT DOCUMENTATION PAGE

READ INSTRUCTIONS BEFORE COMPLETING FORM

1. REPORT NUMBER: RADC-TR-79-45 (19) TR-79-45
2. GOVT ACCESSION NO.
3. RECIPIENT'S CATALOG NUMBER

4. TITLE (and Subtitle): HIGH POWER MILLIMETER WAVE AMPLIFIER
5. TYPE OF REPORT & PERIOD COVERED: Interim Report 2, 31 Mar 78 - 1 Nov 78
6. PERFORMING ORG. REPORT NUMBER: N/A

7. AUTHOR(s): S. Heji, R. Morwood, A. Jory, A. Nordquist, A. Karp, R. Symons (Howard / Jory)
8. CONTRACT OR GRANT NUMBER(s): F30602-78-C-0011, ARPA Order-3492

9. PERFORMING ORGANIZATION NAME AND ADDRESS: Varian Associates, Inc. Palo Alto Microwave Tube Div, 611 Hansen Way, Palo Alto CA 94303
10. PROGRAM ELEMENT, PROJECT, TASK AREA & WORK UNIT NUMBERS: 62301E, C1920004, 00

11. CONTROLLING OFFICE NAME AND ADDRESS: Defense Advanced Research Projects Agency, 1400 Wilson Blvd, Arlington VA 22209
12. REPORT DATE: April 1979
13. NUMBER OF PAGES: 74

14. MONITORING AGENCY NAME & ADDRESS (if different from Controlling Office): Rome Air Development Center (OCTP), Griffiss AFB NY 13441
15. SECURITY CLASS. (of this report): UNCLASSIFIED
15a. DECLASSIFICATION/DOWNGRADING SCHEDULE: N/A

16. DISTRIBUTION STATEMENT (of this Report): Approved for public release; distribution unlimited.

(9) Interim rept. no. 2, 31 Mar - 1 Nov 78

17. DISTRIBUTION STATEMENT (of the abstract entered in Block 20, if different from Report): Same

(12) 69 pp

18. SUPPLEMENTARY NOTES: RADC Project Engineer: 1/Lt Kevin O'Brien (OCTP)

19. KEY WORDS (Continue on reverse side if necessary and identify by block number)

Gyrotron
Gyroklystron
Gyro-TWT
Microwave Tube
Cyclotron Resonance Maser
Cyclotron Harmonic Operation
Millimeter Wave Amplifier

20. ABSTRACT (Continue on reverse side if necessary and identify by block number)

This report describes a TE_{11}^{o} gyro-TWT which has been built and tested and has shown net gain. Supporting computational effort is described as is work on higher impedance circuits. Also included is a review of progress on harmonic gyro-klystrons built during Phase I and tested during Phase I and the early part of Phase II.

DD FORM 1 JAN 73 1473

UNCLASSIFIED

SECURITY CLASSIFICATION OF THIS PAGE (When Data Entered)

406 552

slt

TABLE OF CONTENTS

Section		Page
I.	INTRODUCTION	1
II.	HISTORY OF THE PHASE I AMPLIFIER: VGX-8080 S/N 1	3
III.	DESIGN OF THE GYRO-TWT	7
IV.	TEST OF THE GYRO-TWT	10
V.	REBUILD OF THE GYRO-TWT: VGC-8160 S/N 1R	14
VI.	SMALL-SIGNAL GAIN CALCULATIONS	15
VII.	THE CYLMAS COMPUTER PROGRAM	29
	The CYLMAS Computer Program at Varian	29
	Incompatible Features	30
	Program Modifications	30
	Program Changes	31
	Standard and Non-Standard Subprograms	32
VIII.	HIGH IMPEDANCE CIRCUIT CALCULATIONS	33
	Introduction	33
	Predictions	33
	Conclusions	45
	Implementation	45
IX.	CONCLUSIONS AND PLANS	47
APPENDIX CYLMAS		50
REFERENCES		65

LIST OF ILLUSTRATIONS

Figure		Page
1.	Waveguide Dispersion with Oscillation Beam Lines.....	11
2.	Axial Field -- VGC-8160 Solenoid.....	12
3.	Gyro-TWT Dispersion Relation for Ω_o/ω_c = 1.05 $P_\perp/P_\parallel$ = 1.....	16
4.	Gyro-TWT Dispersion Relation for Ω_o/ω_c = 1.07 $P_\perp/P_\parallel$ = 1.....	17
5.	Gyro-TWT Dispersion Relation for Ω_o/ω_c = 1.10 $P_\perp/P_\parallel$ = 1.....	18
6.	Gyro-TWT Dispersion Relation for Ω_o/ω_c = 1.25 $P_\perp/P_\parallel$ = 1.....	19
7.	Gyro-TWT Dispersion Relation for $\Omega o/\omega_c$ = 1.50 $P_\perp/P_\parallel$ = 1.....	20
8.	Gyro-TWT Dispersion Relation for Ω_o/ω_c = 1.05 $P_\perp/P_\parallel$ = 2.....	21
9.	Gyro-TWT Dispersion Relation for Ω_o/ω_c = 1.07 $P_\perp/P_\parallel$ = 2.....	22
10.	Gyro-TWT Dispersion Relation for Ω_o/ω_c = 1.10 $P_\perp/P_\parallel$ = 2.....	23
11.	Gyro-TWT Dispersion Relation for Ω_o/ω_c = 1.25 $P_\perp/P_\parallel$ = 2.....	24
12.	Gyro-TWT Dispersion Relation for Ω_o/ω_c = 1.50 $P_\perp/P_\parallel$ = 2.....	25
13.	Spatial Growth Rate -- Ω_o/ω_c = 1.05 $P_\perp/P_\parallel$ = 2.....	27
14.	Spatial Growth Rate -- Ω_o/ω_c = 1.05 $P_\perp/P_\parallel$ = 1.....	28
15.	Transmission Line with Periodic Loading and Increase Transversee Impedance.....	34
16.	Brillouin-Type Diagram for Transmission Line with Periodic Loading by Either Lumped Series Inductances or Shunt Capacitances; Case 1, constant ratio of B to Y_o or X to Z_o.....	36

LIST OF ILLUSTRATIONS (CONT.)

Figure		Page
17.	Normalized Transverse Impedance or Admittance Predictions for Case of Figure 16, Evaluated Midway Between Loading Elements.....	37
18.	Normalized Transverse Impedance or Admittance Predictions for Case of Figure 16, Evaluated in Plane of Loading Element.....	39
19.	Brillouin-Type Diagram for Transmission Line with Periodic Loading by Either Lumped Series Inductances or Shunt Capacitances; Case 2, ratio B/Y_o or X/Z_o is Proportional to Electrical Length ϕ.....	40
20.	Normalized Transverse Impedance or Admittance Predictions for Case of Figure 19, Evaluated Midway Between Loading Elements.....	41
21.	Normalized Transverse Impedance or Admittance Predictions for Case of Figure 19, Evaluated in Plane of Loading Element.....	42
22.	Brillouin-Type Diagram for Corrugated Transmission Line.....	43
23.	Normalized Transverse Impedance or Admittance Predictions for Cases of Figure 22.....	44
24.	Milestone Chart.....	49

I. INTRODUCTION

The objective of this program is to design a high power pulsed amplifier for millimeter wave operation. Desired operating characteristics are:

center frequency	94 GHz
electronic bandwidth	> 4%
peak power	100 kw
average power	10 kW
beam efficiency	30%
power gain	30 dB

The development is limited to the consideration of gyrotron-type amplifiers which involve an interaction based on cyclotron resonance.

The present program was preceded by a Phase I study effort[1] which explored the feasibility of gyroklystron amplifiers with cyclotron harmonic operation. As part of the study effort, a three-cavity gyroklystron amplifier operating on the second harmonic of the cyclotron frequency at X-band was built and partially tested.

The first interim report for Phase II[2] covered the completion of testing of the X-band gyroklystron built under the previous study program. Measurements of saturated output power were included in the report. Spectrum measurements and noise figure measurements were also presented.

In addition, the report contained a discussion of the alternatives which were considered for converting the three-cavity gyroklystron to the gyro-TWT.

This report describes results on the first TE_{11} mode gyro-TWT experiment which demonstrated some net gain. The gain figures were somewhat lower than expected due to large launching losses. At the end of this reporting period, the tube had been rebuilt with an increased length and was essentially ready for test.

II. HISTORY OF THE PHASE I AMPLIFIER: VGX-8080 S/N 1

The amplifier constructed in Phase I was a three-cavity gyroklystron, for operation at 10.35 GHz. It was designed to operate at the second harmonic of the cyclotron resonance. The resonance condition is given by the equation

$$\omega = \frac{neB}{\gamma m_o} \qquad (1)$$

where ω is the operating frequency, B is the axial dc magnetic field, e/m_o is the charge-to-mass ratio of the electron, γ is the relativistic mass factor, and n is the harmonic number. Operation at the second harmonic of the resonance allows the magnetic field to be smaller by a factor of two.

The operating parameters for the 10.35 GHz amplifier are given in Table I. Additional information on the design is included in the final report for Phase I[1].

Initial operation resulted in the observation of a microwave gain of 9 to 10 dB under small signal conditions where the power output was about 100 w peak. This operation was achieved at reduced beam voltage of 40 kV. Amplifier operation at higher beam voltage had been prevented by interfering oscillations involving the TE_{111} resonance in the input cavity interacting with the fundamental cyclotron resonance condition. The oscillation occurred at a frequency near 5.4 GHz and was somewhat tunable depending on main magnetic field values. Table 2 shows a summary of preliminary test values compared to design values.

At the start of Phase II, a linear-beam klystron capable of about 8 kw peak output power was installed as a driver for the gyroklystron, allowing the gyroklystron to be driven to saturation. The highest values of saturated power, small signal gain, and efficiency are listed in Table 3. Curves relating the tube performance to the available parameters, beam voltage and current, anode voltage, and magnetic field, can be found in the previous interim report.[2]

PRECEDING PAGE NOT FILMED
BLANK

TABLE 1

10.35 GHz AMPLIFIER DESIGN VALUES

1.	Power output - peak	100	kw	
	average	5	kW	
2.	Gain	30	dB	
3.	Bandwidth	0.1	%	
4.	Magnetic field	1.96	kg	
5.	RF circuits (TE_{011} cavities)			
	Input cavity length	1.5	λ	*
	First drift length	1.2	λ	
	Center cavity length	1.5	λ	
	Second drift length	1.2	λ	
	Output cavity length	3	λ	
	Cavity loaded Q (each cavity)	1000		
	Drift tube radius (0.51)	0.58	in	
6.	Beam			
	Voltage	60	kV	
	Current	5	A	
	Outer beam radius	0.53	in	
	Inner beam radius	0.19	in	
	Axial velocity	0.2	c	**
	Transverse velocity	0.4	c	
	Electron orbit radius	0.15	in	

* λ = Free-space wavelength at the operating frequency

** c = velocity of light

TABLE 2

SUMMARY OF PRELIMINARY TEST RESULTS

Parameter	Design Value	Preliminary Test Value
Beam voltage	60 kV	40 kV
Gun anode voltage	31 kV (52%)	24 kV (60%)
Beam current	5 A	4.5 A
Main magnet field	1960 g	1960 g ± 5%
Gun magnet	485 g	450 g ± 10%
Microwave gain	23-26 dB	9-10 dB
Peak body current	0	80 ma
Peak gun anode current	0	<4 ma

TABLE 3

BEST PERFORMANCE

Parameters	Test Value
Beam voltage	50 kV
Beam current	5.0 A
Saturated power	20.56 kW
Small signal gain	5.8 dB
Gain compression	1.4 dB
Saturated efficiency	8.2%

III. DESIGN OF THE GYRO-TWT

The gyro-TWT version of the family of cyclotron resonance masers differs from the klystron or monotron by virtue of its non-resonant rf circuit. The beam is well-coupled to the EM fields over a reasonable bandwidth (5-10%). Unlike a conventional (linear beam) TWT, the gyro-TWT utilizes a fast-wave interaction between circuit and beam. This allows the use of simple, non-periodic rf circuits.

To minimize development time and cost it was decided to design gyro-TWT experiments using the gyroklystron hardware from Phase I wherever possible. In particular, the existing solenoid and gun designs were to be used.

The gyro-TWT was designed to employ the TE_{11} mode in a circular guide and to operate at the fundamental cyclotron resonance, about 5.2 GHz. (10.35 GHz fundamental operation is beyond the capability of the existing solenoid.) The input coupling system had to fit within the magnet bore, which was difficult at 5.2 GHz with conventional rectangular waveguide components. An attempt was made to couple to the rf circuit using a coaxial transmission line terminated in a probe or loop. The close proximity of the beam to the wall of the interaction circuit required the use of small loops or probes which had high radiation resistances, and required excessive impedance transformation to achieve an acceptable match. A hybrid solution was found involving coupling to the circuit with a rectangular waveguide port and then using a vacuum tight coax-to-waveguide transition. The matching for the rectangular guide to the interaction circuit required a capacitance at the junction. Since two orthogonal TE_{11} modes can exist, two inputs were required separated 90° azimuthally.

When the rf circuit assemblies were completed, testing of the entire circuit revealed an input match significantly worse than the cold test measurements predicted. Attempts were made to analyze the mismatch using Smith Chart impedance measurements across the 10% band. The results showed that the best place for a broadband improvement of the match occurred at a plane located inside the coaxial elbow - vacuum window assembly. The addition of reactive

elements to the coaxial elbow assembly yielded a match better than 2:1 over a 6% band.

For the gyro-TWT experiment, using the TE_{11} mode, a change in the output window design was required. The previous window design had an axial break in the guide wall suitable for the TE_{01} mode and was matched for operation at 10.35 GHz. For use with TE_{11} mode, the axial wall gap had to be removed, and the window thickness increased to obtain a C-band match. Transmission measurements on the window revealed several trapped window modes above the band, with the lowest at the upper band edge. These should not be troublesome..

Table IV shows the design values for the gyro-TWT. The rf circuit length was determined primarily by the size of the available magnet. The uncertainties in the values for output power and gain reflect the unknown character of the launching losses and the lack of good gain calculations. The rf circuit was capable of propagating two orthogonal TE_{11} modes which were sure to be coupled somewhat by the rotating beam; making the launching losses difficult to predict. At the time the tube was built, the NRL computer codes for TWT gain had not yet been transferred to Varian (see Section VII).

TABLE 4

5.2 GHz GYRO-TWT DESIGN VALUES

1.	Power Output - peak	~100	kw
	- average	~ 5	kW
2.	Gain	~20-30	dB
3.	Bandwidth	5.0	%
4.	Magnetic field	1.96	kG
5.	RF Circuit (circular waveguide)		
	Guide length	5.1	λ*
	Guide radius	0.72	in
6.	Beam		
	Voltage	60	kV
	Current	5	A
	Outer beam radius	0.53	in
	Inner beam radius	0.19	in
	Axial velocity	0.2	c**
	Transverse velocity	0.4	c
	Electron orbit radius	0.15	in

* λ = Free-space wavelength at the operating frequency.

** c = velocity of light (in vacuum).

IV. TEST OF THE GYRO-TWT

The gyro-TWT was tested into a circular waveguide load at a low rf duty (1-2%). A 10 W TWT linear beam amplifier was used to drive one of the two orthogonal inputs while the other was terminated in a matched load. An iris coupled, side wall output coupler in circular guide was used to sample the output in the two orthogonal modes. This output was measured with thermistor mounts and power bridges.

To start, two different oscillations were observed with frequencies near 4.8 and 8.0 GHz respectively. The first oscillation was smoothly tunable between 4.8 and 5.2 GHz and generated a significant amount of power (1-2 kw peak) at the input ports, which suggests it may be either a backward wave oscillation in the TE_{11} mode, or it may be due to match difficulties near the waveguide cutoff. Figure 1 shows the beam line for this oscillation plotted against the TE_{11} and TE_{01} waveguide dispersion hyperbolas for the circuit.

The other observed oscillation consisted of discrete frequencies between 8.05 and 8.55 GHz. The behavior of the oscillation was similar to that of a multi-wavelength, multi-mode cavity which oscillated at separated frequencies depending on the magnetic field value. The beam line for this mode is also plotted in Figure 1, along with its second harmonic beam line, identifying the oscillation as a TE_{21} mode oscillation at the second harmonic of the cyclotron resonance.

The axial magnetic field was adjusted to lie between the values used to obtain the two oscillations. This yielded indications of forward wave gain. After some optimization of magnetic field, and after increasing the output coupling, small signal gain measurements were taken which indicated gains of 0-3 dB across the band (4.9-5.4 GHz).

At this time, concern over the uniformity of the axial magnetic field motivated removing the tube from the socket and measuring the dc field. With all main magnet sections excited with equal currents, the axial field varied only 1.5% over a 9" length (total rf circuit length is 11"). Figure 2 shows a

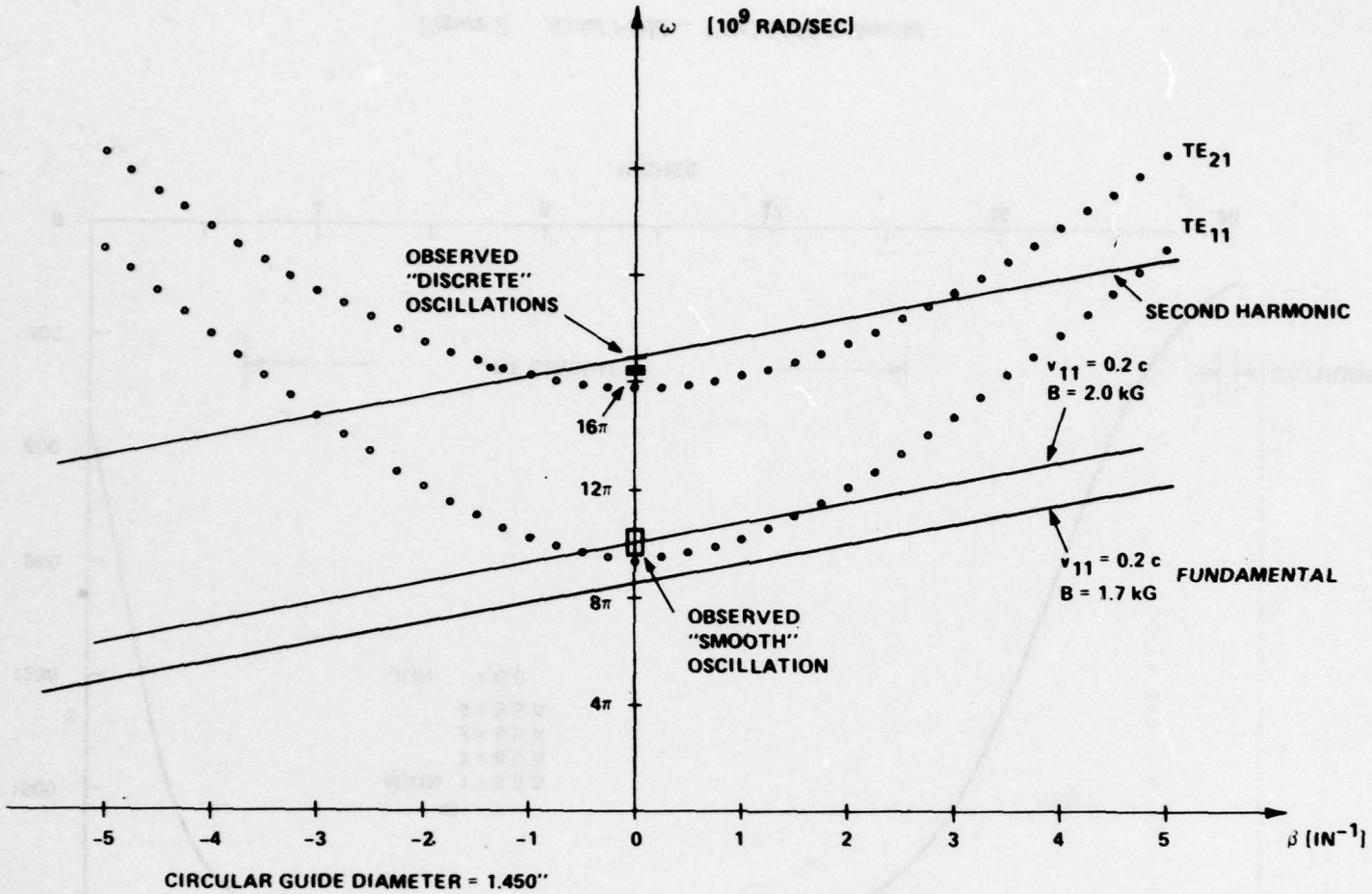

Figure 1. Waveguide Dispersion with Oscillation Beam Lines

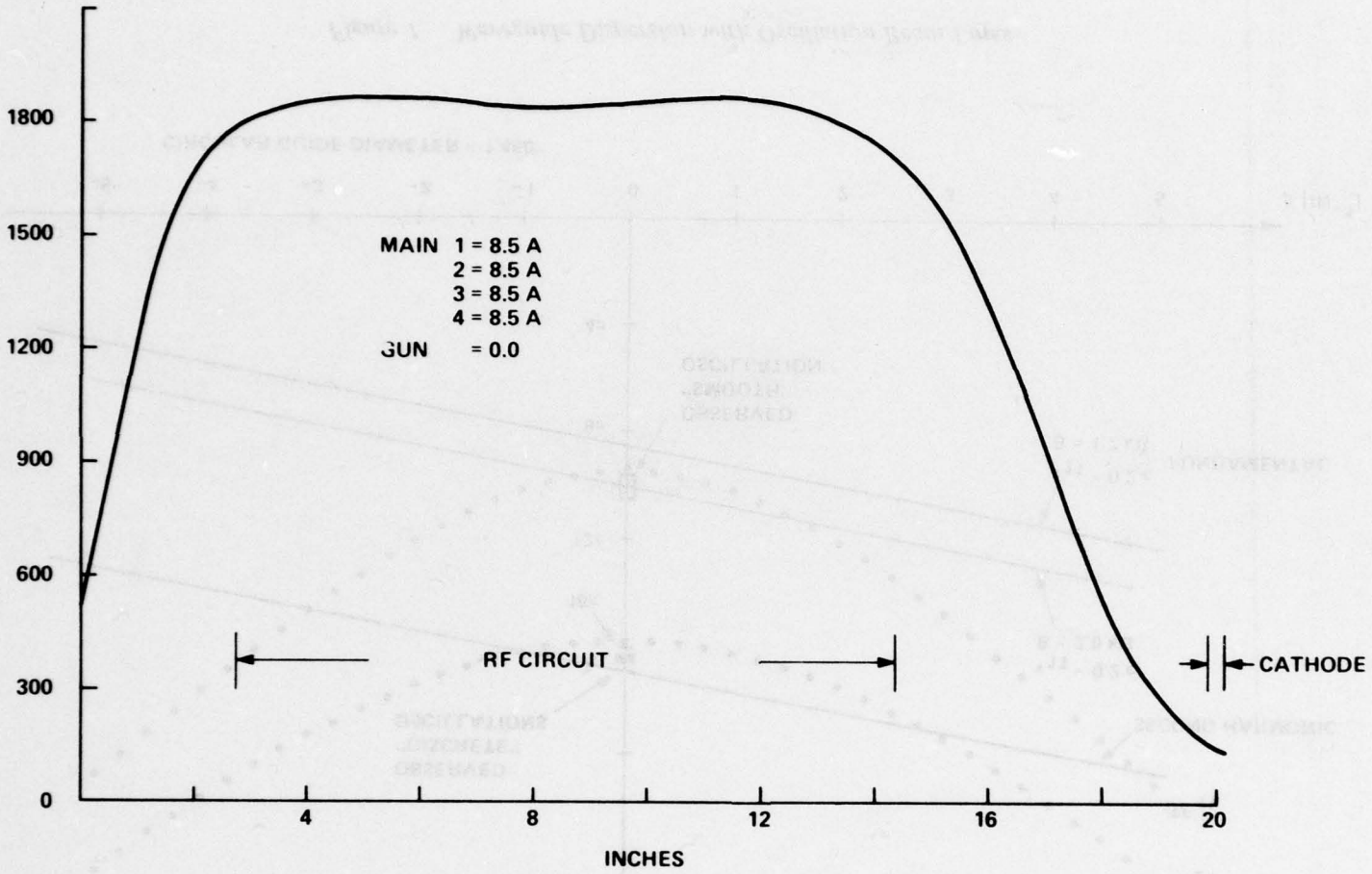

Figure 2. Axial Field – VGC-8160 Solenoid

plot of this field. A measurement of the off axis field at the average beam diameter yielded similarly good results. Because no magnetic problems were found and because calculations indicated that the gain would not exceed the estimated launching loss by any large amount, tests were halted and work was begun on a rebuild.

V. REBUILD OF THE GYRO-TWT: VGC-8160 S/N 1R

From the test results described in the previous section, it was concluded that the tube had only enough gain to overcome the estimated launching losses. Accordingly, a center section was designed which could be added to the tube and effectively double its interaction region. This assembly has been built and incorporated into the device.

A focusing solenoid of increased length was found which will accept the new tube length; and furthermore, is capable of generating higher magnetic fields. This added feature allows us to test the validity of the interaction theory where it concerns changes in magnetic field. This is discussed in the following section.

VI. SMALL-SIGNAL GAIN CALCULATIONS

During the last period, prior to obtaining the NRL CLYMAS program, a BASIC program was written which solves the dispersion relations derived by Sprangle and Drobot[3] for the case of a strip beam in a $TE_{n,o}$ rectangular waveguide and by Chu and Drobot[4] for a hollow cylindrical beam in a $TE_{o,n}^{o}$ mode in a circular waveguide. Both these small signal dispersion relations have the same form with the unperturbed waveguide mode dispersion relation on the left-hand side of the equation and the beam waves on the right-hand side. A coefficient which defines the strength of the coupling between the beam and circuit waves multiplies the left-hand side of the equation. While this coefficient may be written in terms of various parameters, it is equivalent to C in the Pierce analysis and can be written in terms of a circuit impedance and a beam conductance when the rf fields are fairly constant across the orbit diameter of the electrons. For this reason, it is possible to use the dispersion relation for the rectangular $TE_{1,0}$ waveguide case to predict the interaction of our $TE_{1,1}^{o}$ mode tube to a good degree of approximation. This is accomplished by picking the height of a rectangular waveguide so the ratio of the square of the electric field seen by an electron to the power flow in the guide is the same as that for our $TE_{1,1}^{o}$ mode. For interaction with one of the orthogonal pair of $TE_{1,1}^{o}$ modes, the ratio of height to width which satisfies this condition is 1.4. (For interaction with the circularly polarized pair of modes the impedance is twice as great and gains in the subsequent figures should be increased by the cube root of 2.) Figures 3 through 7 show the roots of the dispersion relation for this ratio for various magnetic fields with $p_\perp/p_\parallel$, the ratio of perpendicular to parallel momentum for the electron beam, equal to one. Figures 8 through 12 show the roots with $p_\perp/p_\parallel = 2$. Real roots are shown as solid lines while the real (ω_r) and imaginary (ω_i) parts of complex roots are shown as dotted lines. ω_i is the temporal growth rate. In all figures Ω_o/ω_c is the ratio of the non-relativistic cyclotron frequency to the waveguide cutoff frequency and is the measure of the magnetic field strength.

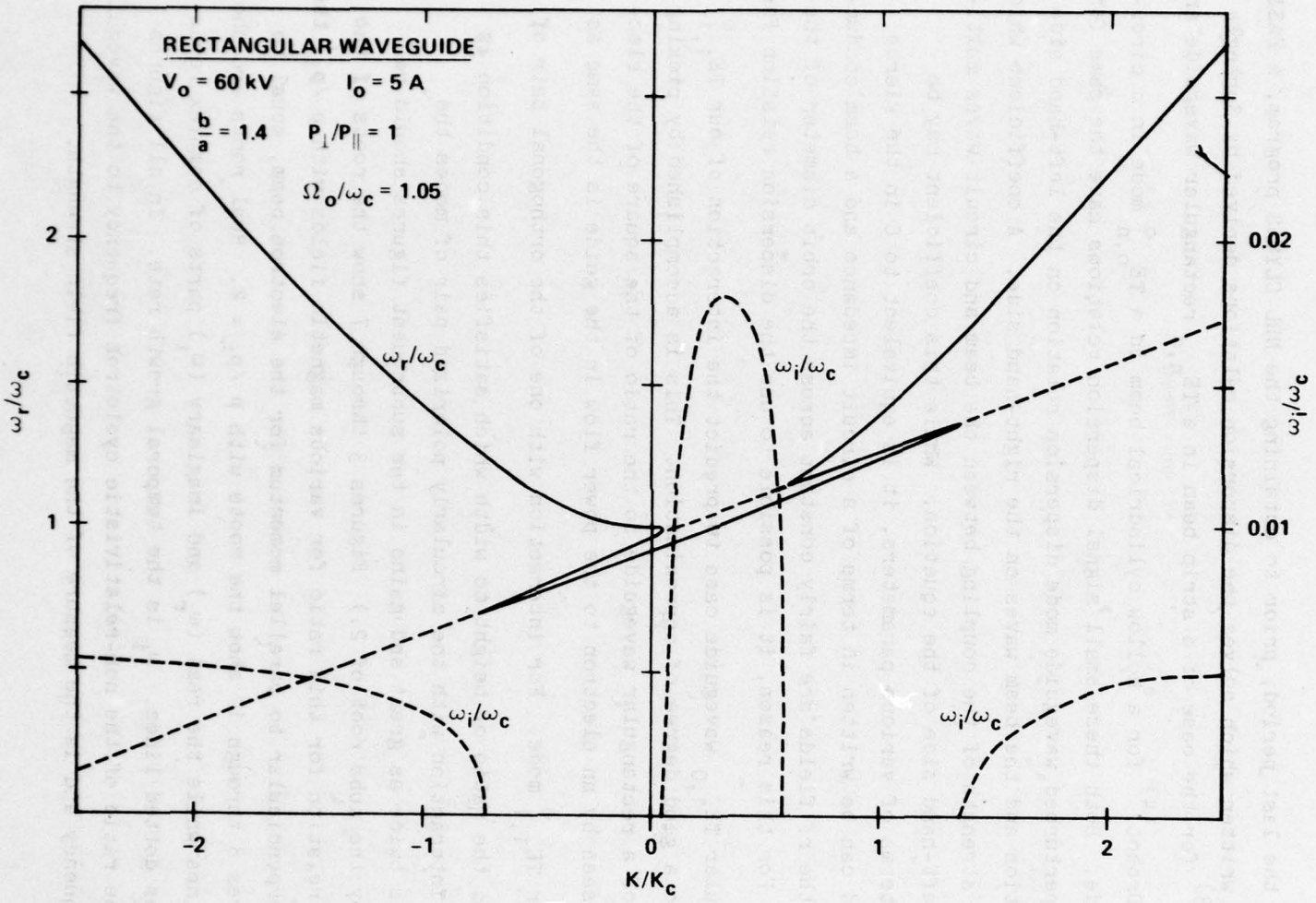

Figure 3. Gyro-TWT Dispersion Relation for $\Omega_o/\omega_c = 1.05$ $P_\perp/P_\parallel = 1$

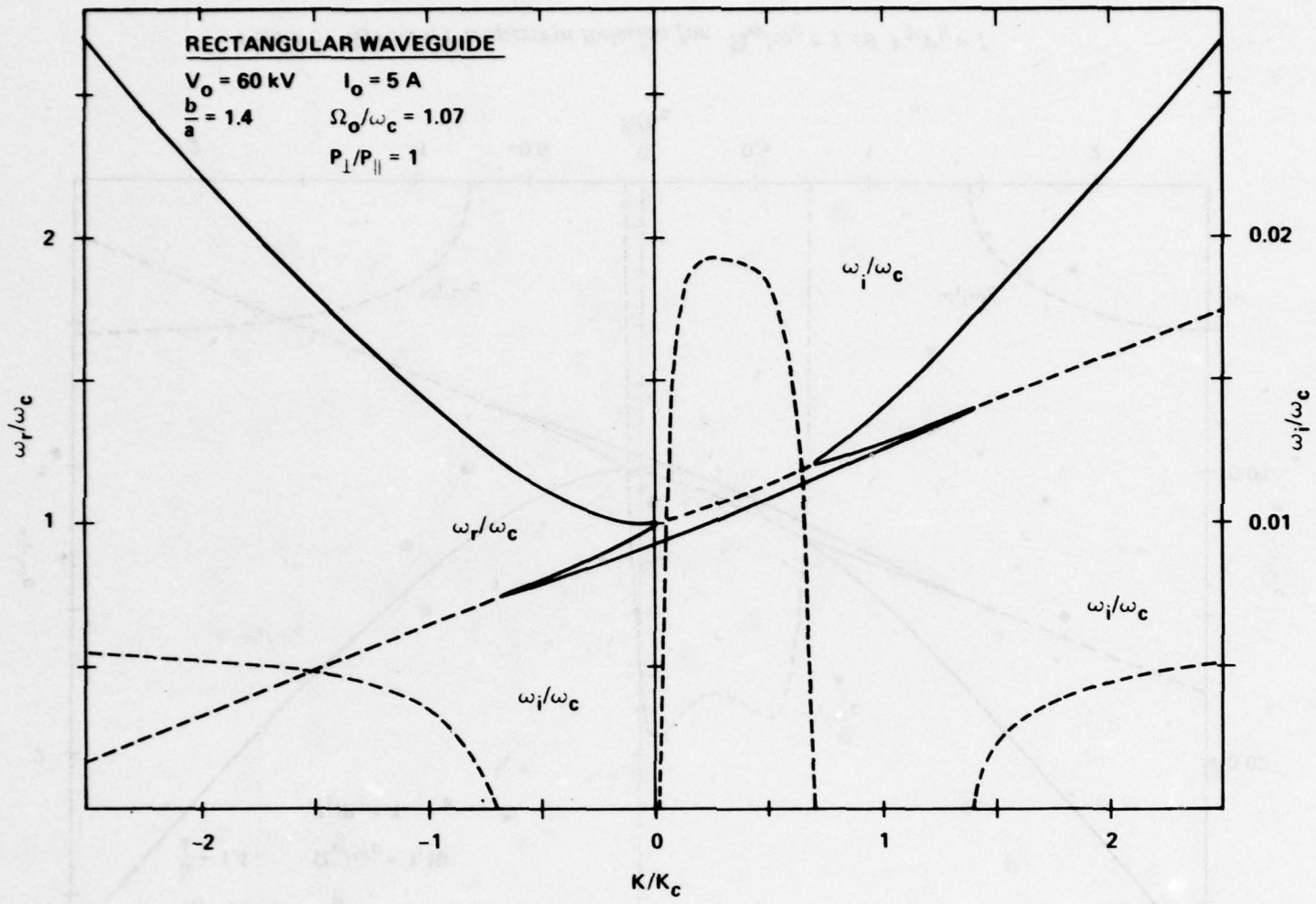

Figure 4. Gyro-TWT Dispersion Relation for $\Omega_o/\omega_c = 1.07$ $P_\perp/P_{||} = 1$

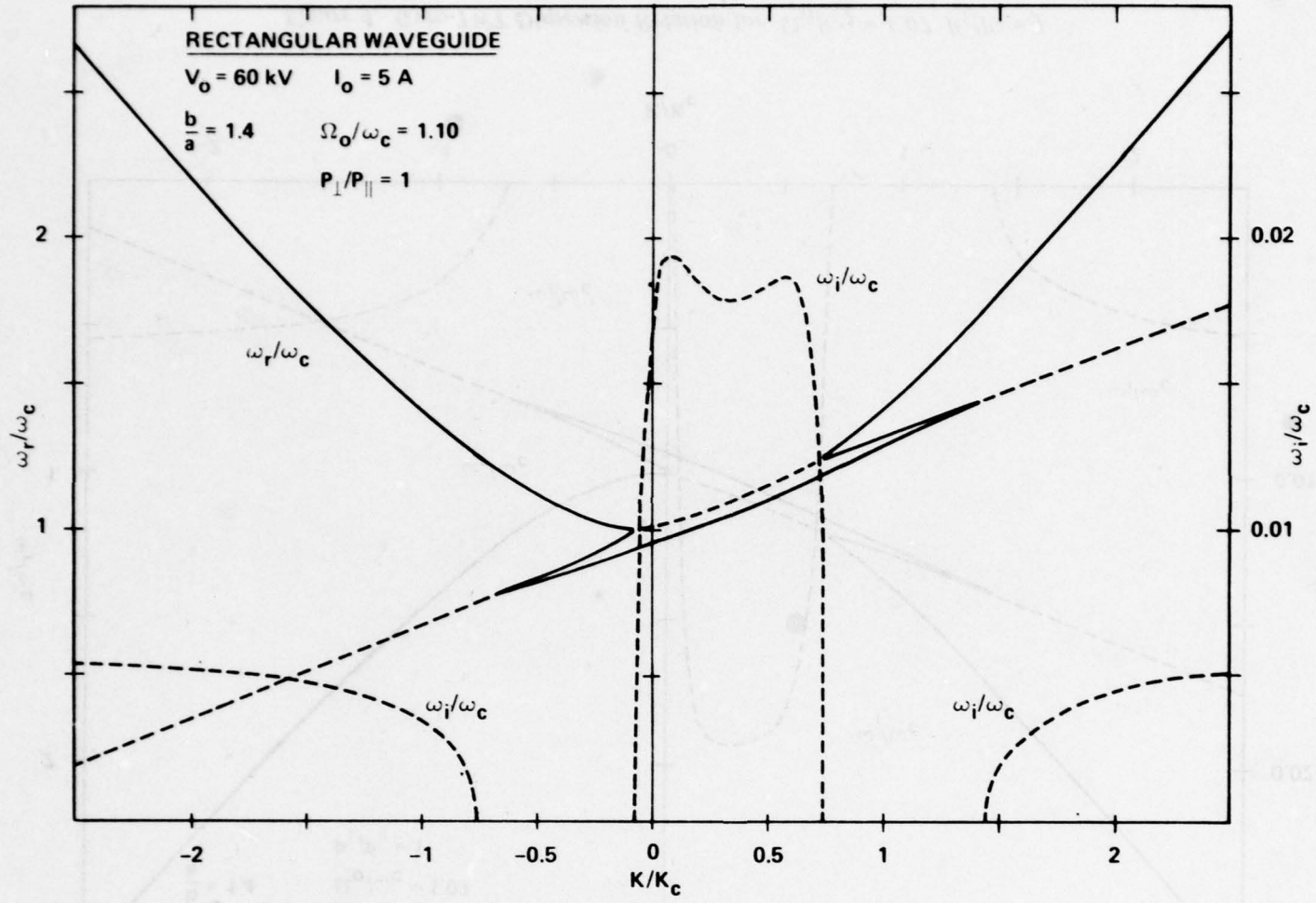

Figure 5. Gyro-TWT Dispersion Relation for $\Omega_o/\omega_c = 1.10$ $P_\perp/P_\parallel = 1$

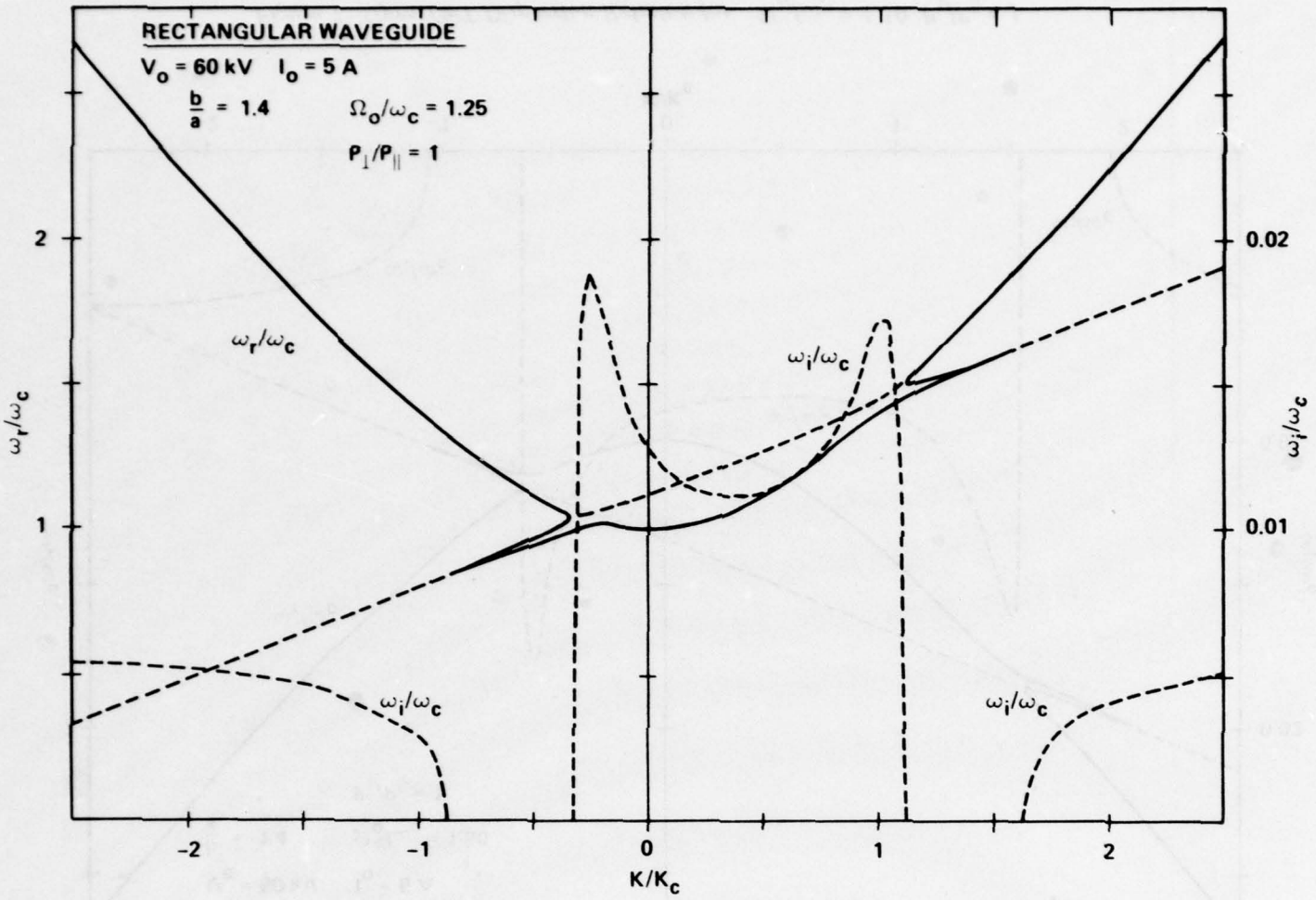

Figure 6. Gyro-TWT Dispersion Relation for $\Omega_o/\omega_c = 1.25$ $P_\perp/P_{||} = 1$

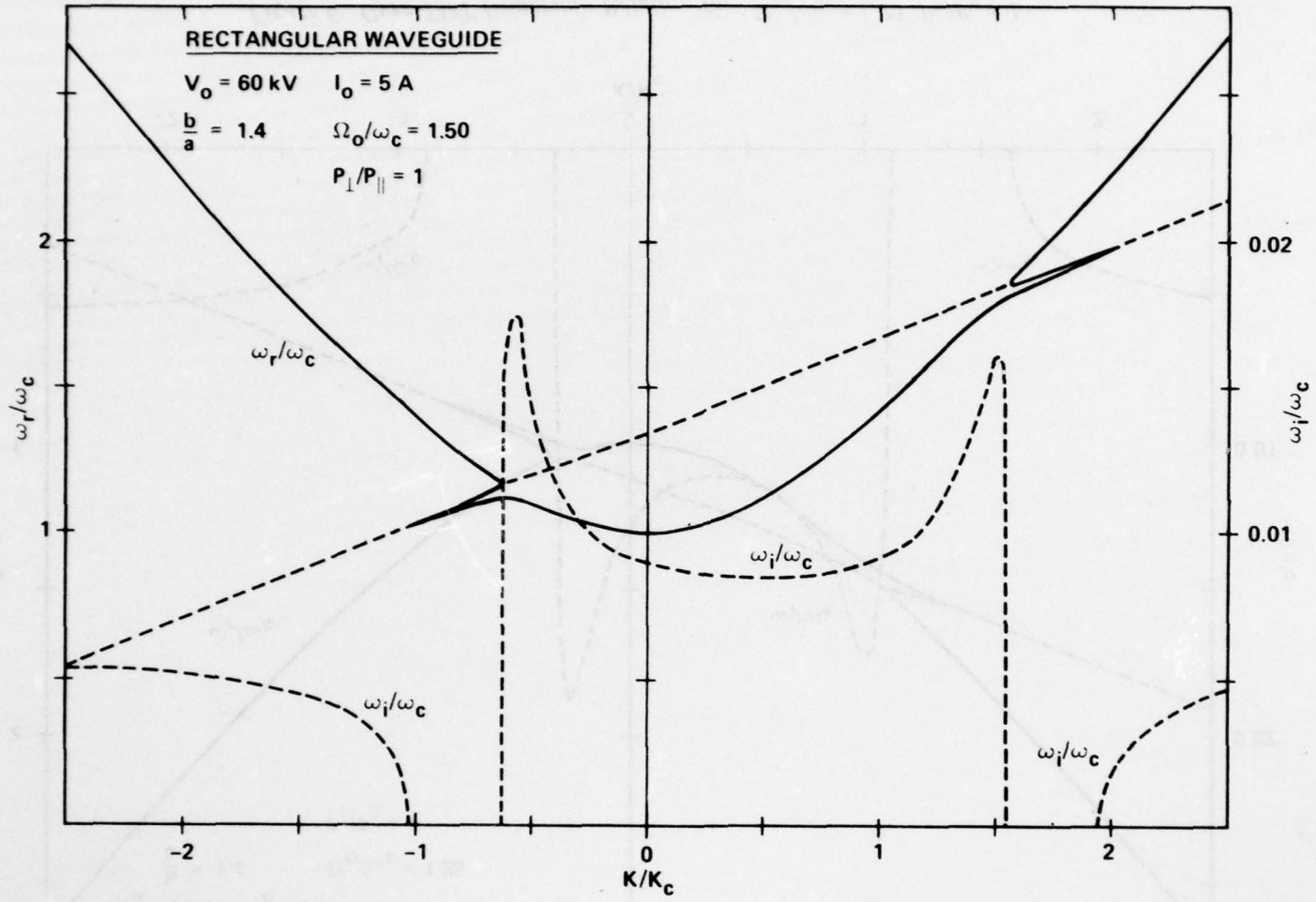

Figure 7. Gyro-TWT Dispersion Relation for $\Omega_o/\omega_c = 1.50$ $P_\perp/P_{||} = 1$

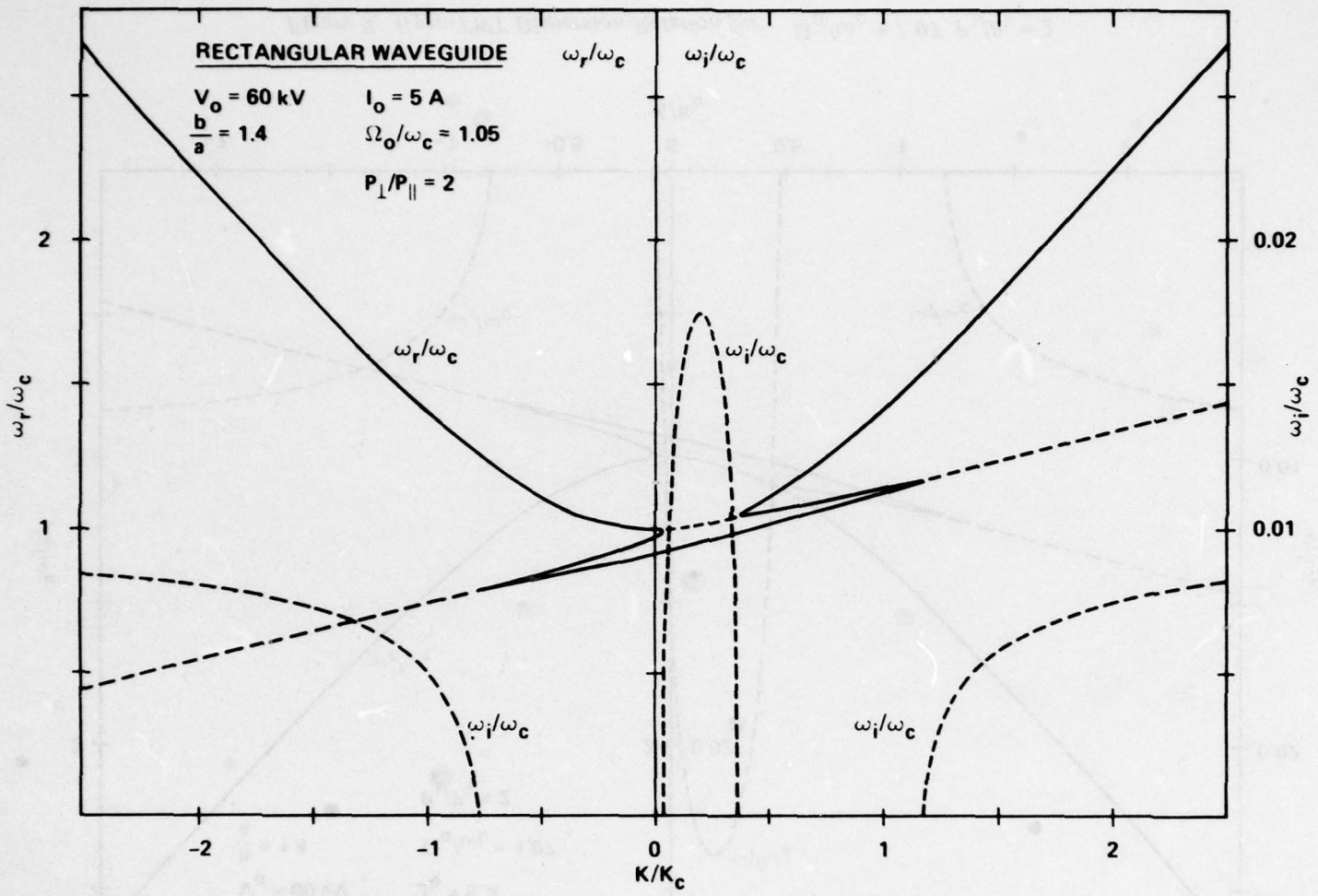

Figure 8. Gyro-TWT Dispersion Relation for $\Omega_o/\omega_c = 1.05$ $P_\perp/P_{||} = 2$

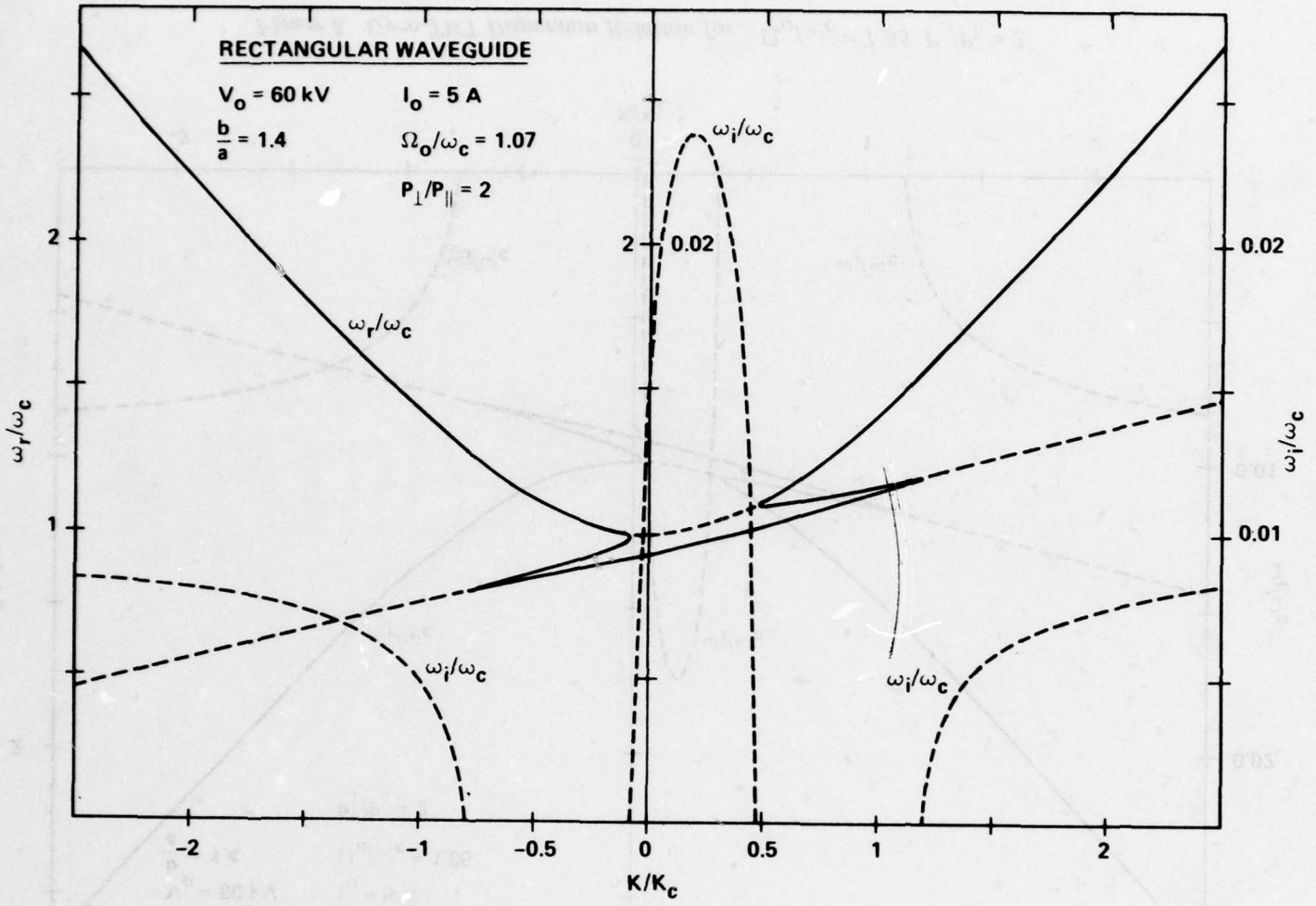

Figure 9. Gyro-TWT Dispersion Relation for $\Omega_o/\omega_c = 1.07$ $P_\perp/P_{||} = 2$

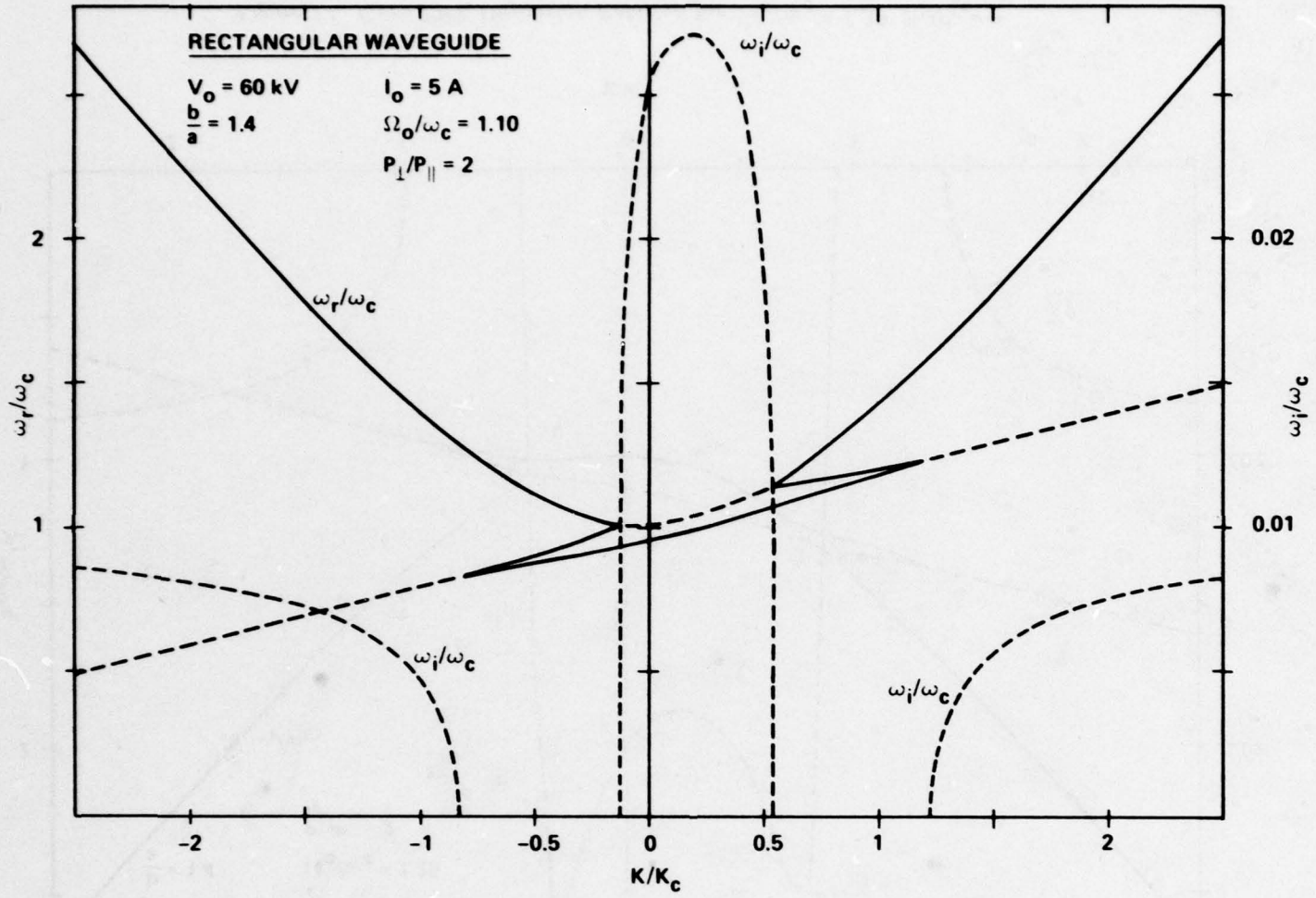

Figure 10. Gyro-TWT Dispersion Relation for $\Omega_o/\omega_c = 1.10$ $P_\perp/P_\parallel = 2$

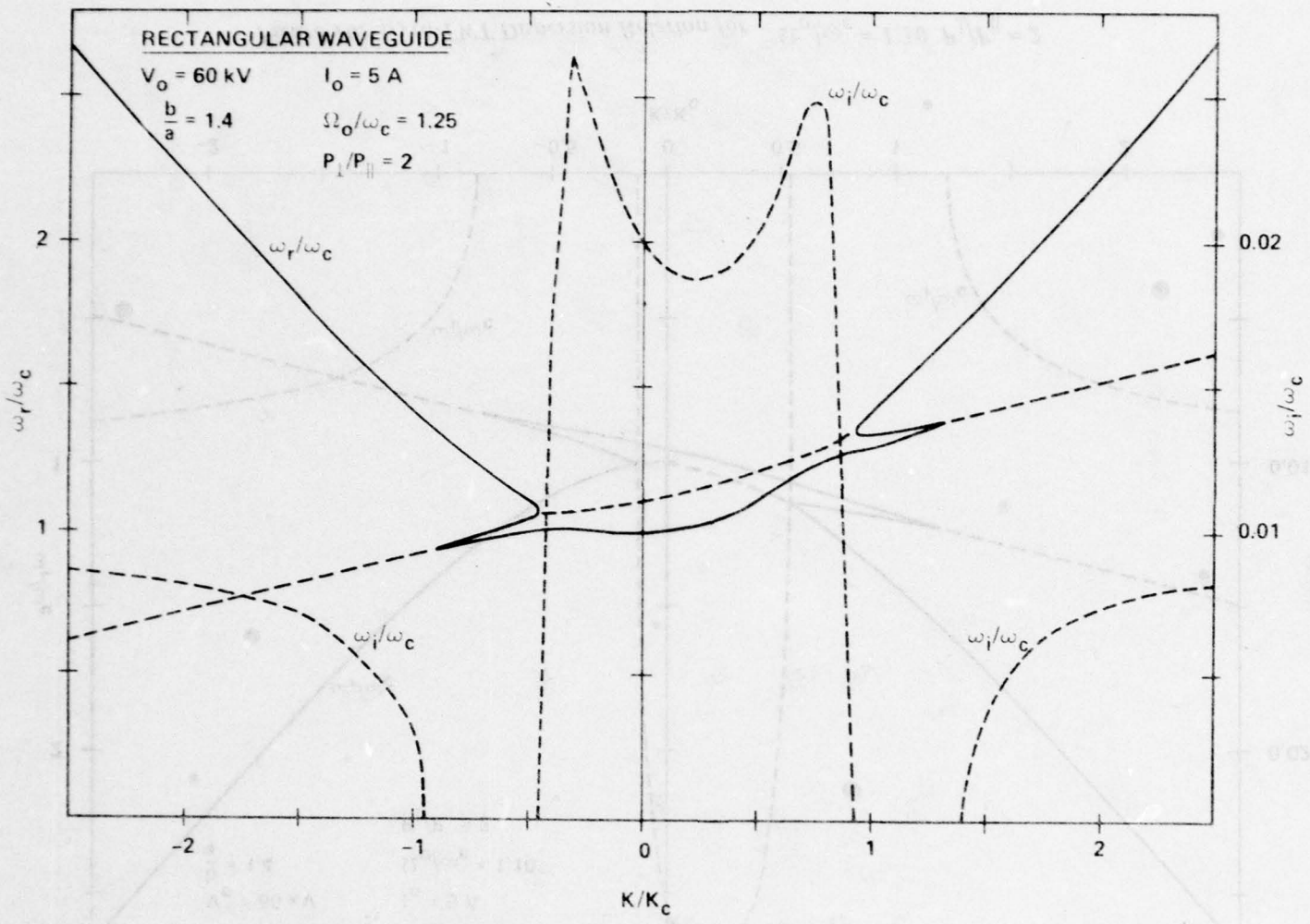

Figure 11. Gyro-TWT Dispersion Relation for $\Omega_o/\omega_c = 1.25$ $P_\perp/P_\parallel = 2$

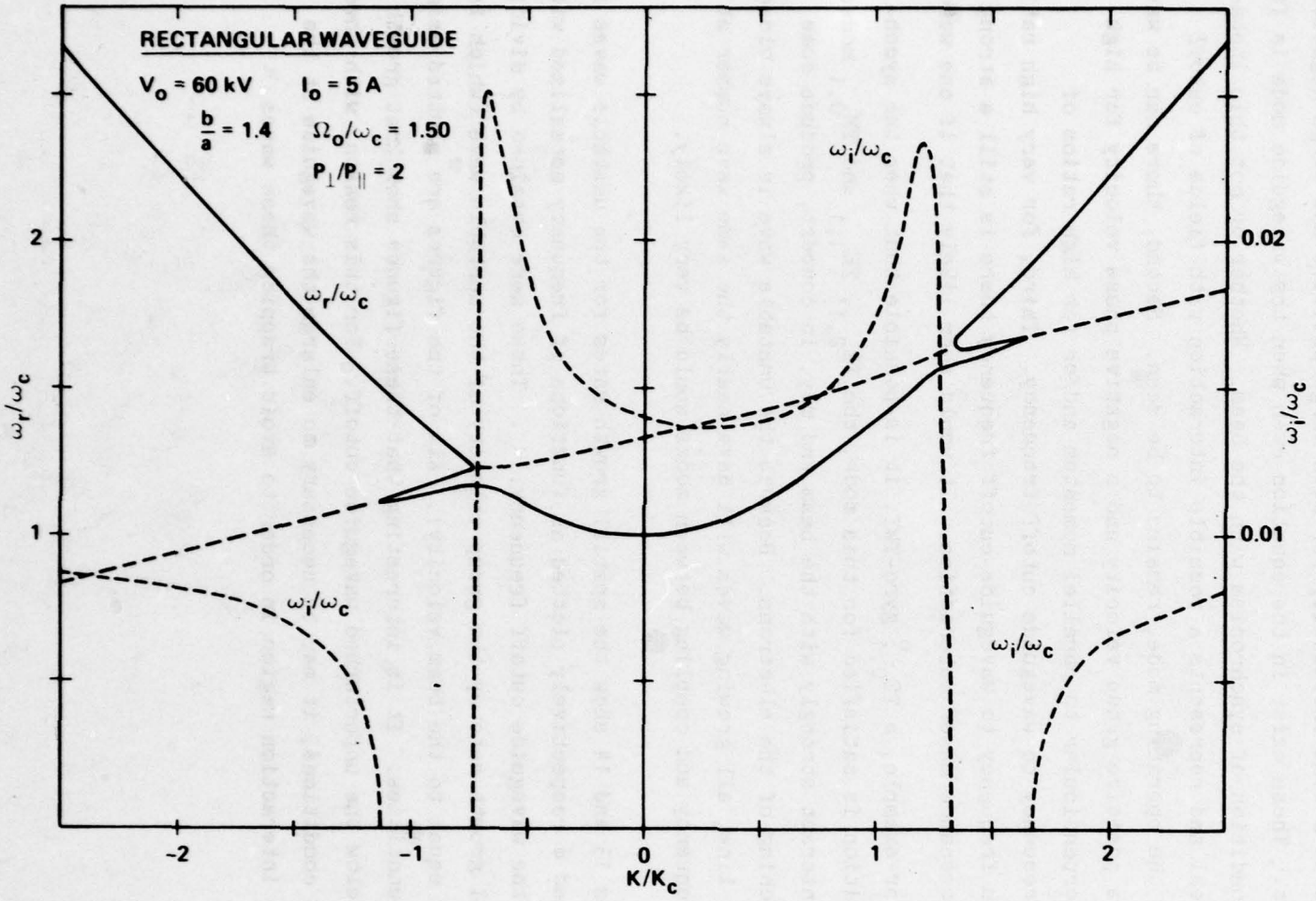

Figure 12. Gyro-TWT Dispersion Relation for $\Omega_o/\omega_c = 1.50$ $P_\perp/P_{||} = 2$

A number of important facts can be seen by examining these figures. First, there is a beam instability for both large positive and large negative wave numbers. These exist in the equation even when the waveguide mode is far above the condition of synchronism with the beam. Whether or not this instability is real and represents a possible interaction with fields of cutoff modes above the operating mode, remains to be seen. Second, there can be waves which have a positive group velocity and a negative phase velocity for high ratios of perpendicular to parallel momentum and/or for high ratios of cyclotron frequency to waveguide cutoff frequency. Third, for very high ratios of cyclotron frequency to waveguide cutoff frequency there is still a strong cyclotron resonance maser interaction. It would seem likely that if one were to build, for example, a $TE^{o}_{0,1}$ gyro-TWT, it is possible that when the synchronism condition is satisfied for this mode, the $TE_{2,1}$, $TE_{1,1}$ and $TM_{0,1}$ modes will also interact strongly with the beam and may, in concert, produce some strange bunching of the electrons. Because the unstable wave is always close to the beam line, all growing waves will have nearly the same wave number at the same frequency and coupling between modes would be very likely.

Figures 13 and 14 show the spatial growth rates for the unstable waves in Figures 3 and 8 respectively plotted as functions of frequency normalized with respect to the waveguide cutoff frequency, ω_c. These were obtained by dividing the temporal growth rate by the group velocity of the unstable wave (which is very nearly equal to the beam velocity). All of the figures are plotted using lab frame quantities. It is interesting that these figures show that growth can exist below the unperturbed waveguide cutoff. For this reason, with these interaction conditions, it may be necessary to enlarge the waveguide at the ends of the interaction region in order to avoid trapping these waves.

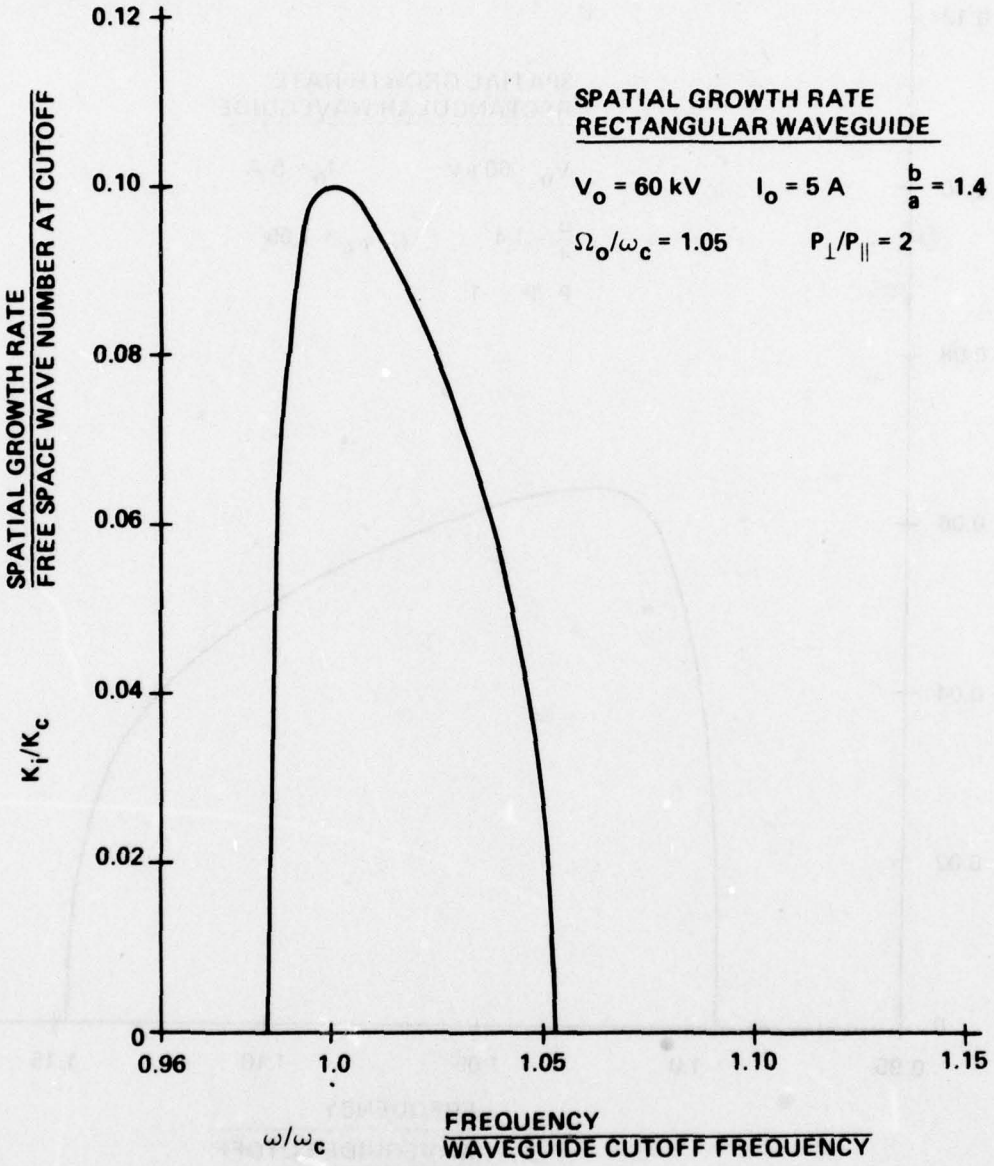

Figure 13. Spatial Growth Rate – $\Omega_o/\omega_c = 1.05$ $P_\perp/P_\parallel = 2$

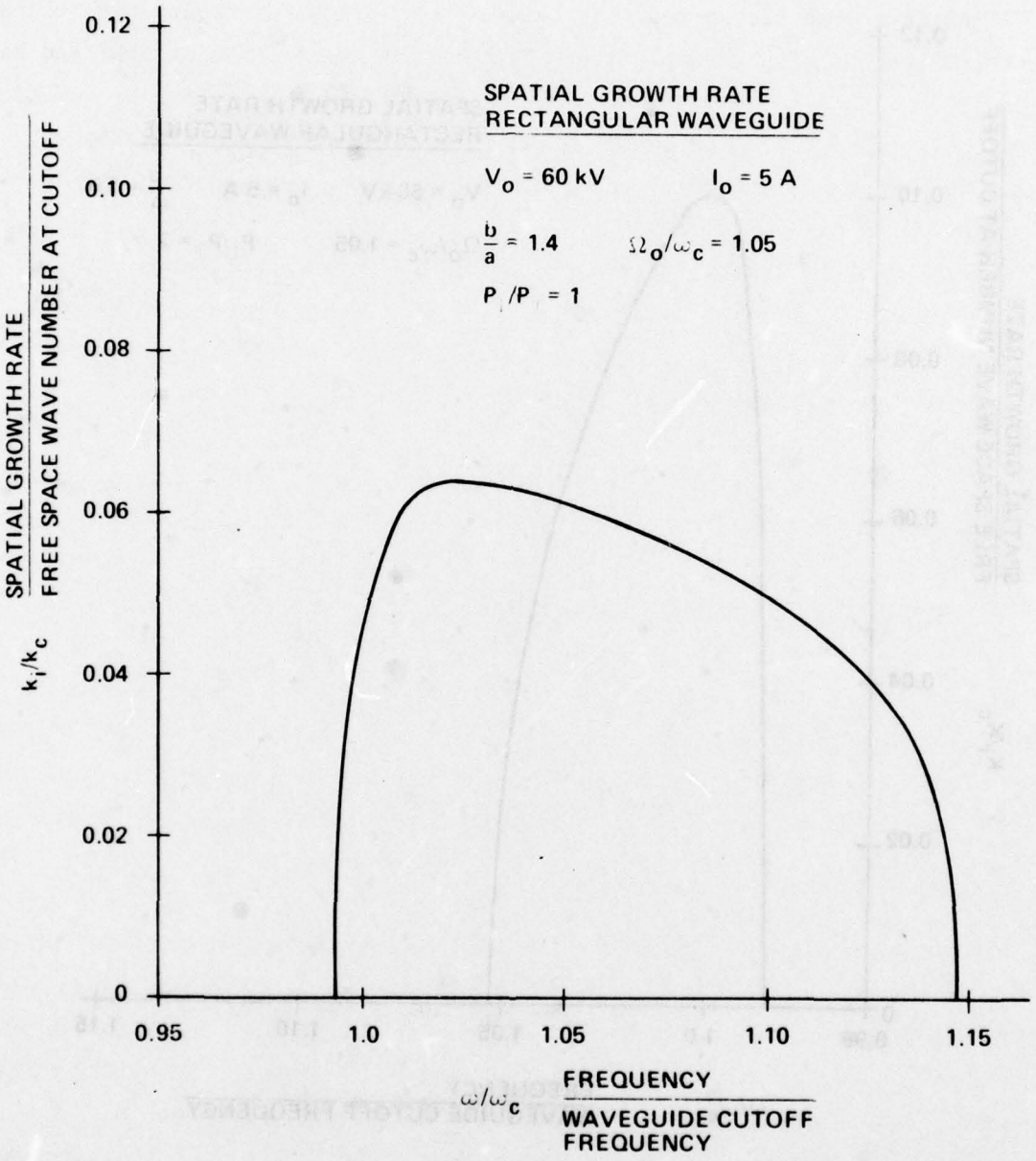

Figure 14. Spatial Growth Rate – $\Omega_o/\omega_c = 1.05$ $P_\perp/P_\parallel = 1$

VII. THE CYLMAS COMPUTER PROGRAM

CYLMAS is a computer program for calculating optimum operating parameters for GYROTRON traveling wave amplifier. The program was written at NRL* and has been modified to operate on the IBM 370/155 computer system at VARIAN. CYLMAS calculates gyrotron traveling wave amplifier performance, neglecting space charge, for cylindrical geometry and for the TE_{0n} waveguide modes.

Users' Documentation of the program at Varian has been prepared. This documentation is primarily a description of the input and output of the computer program plus a minimum of theoretical discussion to aid in preparing input and in understanding program output.

The program is written in FORTRAN IV with the exception of several small subroutines required for plotting which are written in IBM Assembler Language.

THE CYLMAS COMPUTER PROGRAM AT VARIAN

The version of the CYLMAS computer program at Varian can be executed on the Varian computer and will give results identical with those obtained at NRL for a test case supplied by NRL. Users' Documentation of the program has been prepared and should be consulted for detailed information about the program input and output.

Modification of the original program was necessary to permit execution on the Varian computer. From the user's viewpoint the most significant change was a reduction of the number of particles permitted from 1000 to 50 (although work is continuing which will make use of disc storage to restore the ability of the program to handle large numbers of particles). From the programmer's viewpoint, it is important that the subprograms having to do with plotting were

---

* The theoretical basis of the program is described in NRL Memorandum Report 3788 "Theory and Single Wave Simulation of the Gyrotron Traveling Wave Amplifier Operating at Cyclotron Harmonics," K.R. Chu and A.T. Drobot, dated August 1978.

not available and changes were made to allow the program to plot on the CalComp plotter using plotting software at Varian.

INCOMPATIBLE FEATURES

Several features of the program as received made it incompatible with the Varian computer system:

1. The program allowed calculations with up to 1000 particles which exceeded the capacity of the Varian computer. The total number of particles is the number of relativistic mass ratios times the number of different ring radii times the number of particles per ring.

2. The program could store and retrieve for printing and plotting data for up to 28 parameters at up to 2000 cyclotron periods.

3. Some subroutines in the program included ASC fast timescale vector processing.

4. Several of the plotting-connected routines required by the NRL program were not standard CalComp software and were not compatible with Varian proprietary plotting codes.

PROGRAM MODIFICATIONS

In order to execute the program at Varian, the following changes were made:

1. To bring the program within the storage limitations of the Varian computer, a reduction in array sizes was made. Calculation in the Varian version of the program can be made with up to 50 particles.

2. The sizes of the storage arrays were also reduced so that the Varian version of the program can store data for printing and plotting at up to 500 gyrotron periods.

3. All programs now execute without any special vector processing.

4. The program now makes use of Varian-written subroutines for the CalComp plotting.

5. Further modifications are planned. By storing data at the end of each cyclotron period on disk instead of in core, the sizes of the storage arrays can be greatly reduced. Saved core space will be available to again increase the number of particles handled and to include additions to the program in the future, such as calculation including space charge effects or the addition of other waveguide modes.

PROGRAM CHANGES

Changes were made in three phases. The fourth phase is to store data for printing and plotting on disk to be read in at completion of the computation and printed or plotted. This will reduce program size.

Additions to the program to include space charge and to permit calculations with other than the TE_{0n} waveguide modes are planned for the future.

The program ran immediately after reducing array sizes (but with dummy plotting routines). As received, the program required 916K bytes of core storage. The Varian version executed in 240K. Results of a trial computation were identical with the results included with a sample furnished by NRL, except for plotting.

A second round of changes led to duplication of NRL results, including plots made on the line printer.

Finally, additional changes were made and CalComp plots were produced. At the same time some segments of the program were overlaid so that the program now executes in 220K including plot routines.

Users' Documentation was prepared. Description of the input data required by the program and the output produced is contained in the Documentation. Execution time for the sample computation was about 8 min., cpu. The sample computation included 50 particles and 30 cyclotron periods with 50 time steps per period.

STANDARD AND NON-STANDARD SUBPROGRAMS

Names of the subroutines and function subprograms included in the Varian version of the CYLMAS program are included in the Documentation. The language of each subprogram is specified. This Documentation is included as Appendix A to this report.

VIII. HIGH IMPEDANCE CIRCUIT CALCULATIONS

INTRODUCTION

The strength of the interaction in a gyro-TWT depends upon the circuit impedance in much the same way as in a conventional TWT. This circuit impedance is proportional to the ratio of the square of the transverse electric field seen by the beam to the power flow in the guide. One obvious way of obtaining a high circuit impedance is to operate in the dominant waveguide mode as we have done in our present experimental tube. Another way is to use a rectangular or ridged waveguide so the electric field is not strong outside the region occupied by the electron beam. It also seems logical that the impedance of the circuit could be increased by restricting the bandwidth. There is a possibility that this might widen the frequency range over which synchronism is achieved and improve the hot bandwidth of gyro-TWTs. We recognize that the use of periodic circuits would remove one of the attractions of gyro-TWTs; that is, the use of large simple circuits. However, if the dimensions can be kept large enough and the performance potential is interesting enough, the use of periodic circuits may be justifiable. We have therefore made some computations to determine the feasibility of the use of such circuits in gyro-TWTs.

PREDICTIONS

The calculations which will be described were made for a parallel-strip transmission line. However, the analytical work will be presented so as to permit the results to apply also to a rectangular or a ridged rectangular waveguide. Figure 15(a) indicates a succession of narrow slits, each cut so as to introduce a series inductance into the transmission line. Figure 15(b) indicates a widening of the slits to about half the period of the loading. Figure 15(c) indicates that the slots have been enlarged further so that only thin partitions remain. In all cases, an increase in transverse impedance occurs at the center of the region between the inductances, i.e., where the metal conductors approach one another most closely. (A longitudinal impedance develops at the position of an inductance, hence the transverse impedance is diminished there.) Of course, the periodic alterations of the original transmission line produce a low-pass filter (overlooking any lower cutoff if a

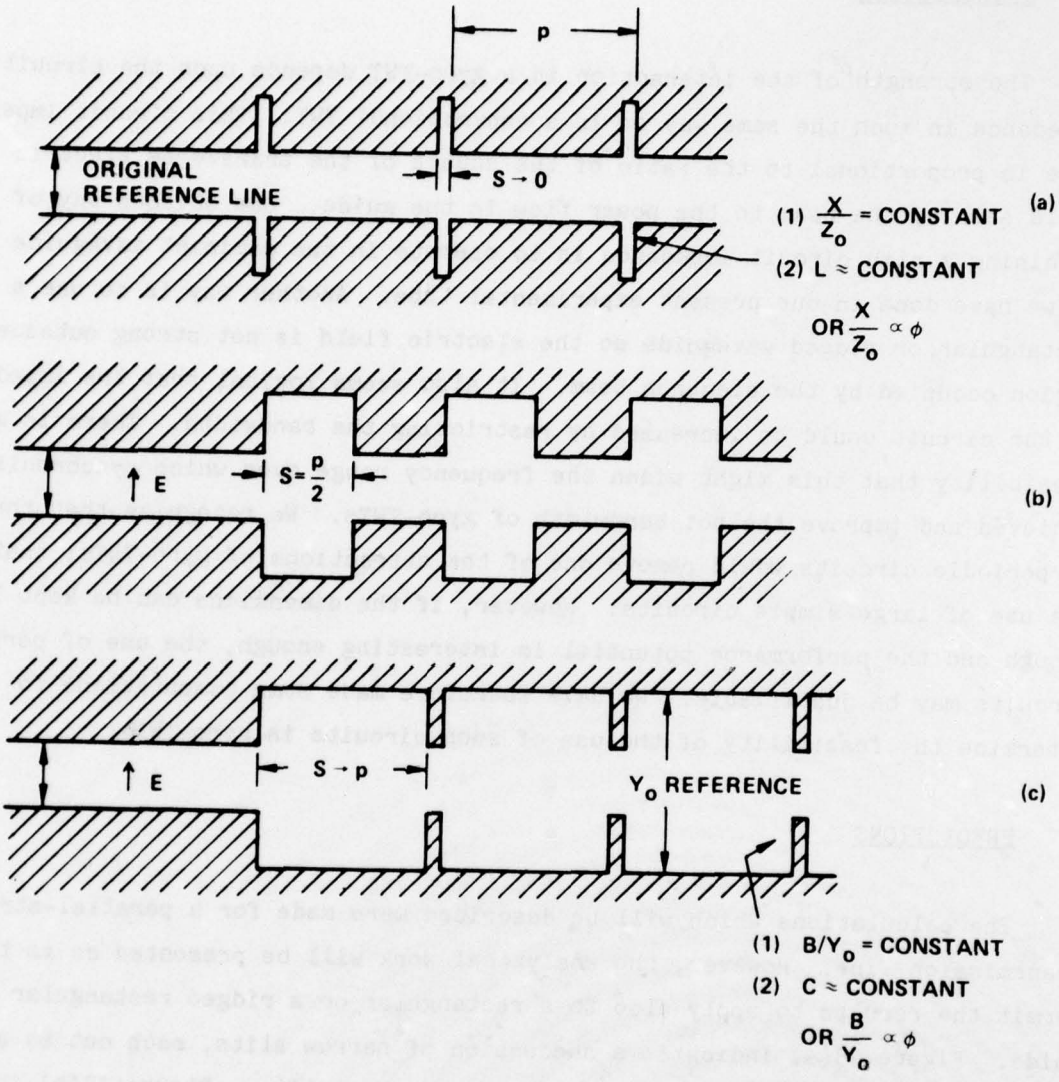

Figure 15. Transmission Line with Periodic Loading and Increase Transverse Impedance

waveguide is used), hence the effects of interest occur at frequencies close to the upper edge of the filter passband.

The case of Figure 15(a) is analyzed as a transmission line for which $Z_o \equiv 1/Y_o = 1$, with localized series loading reactances, X. Two subcases are considered. In Case 1, we assume $X/Z_o \equiv x$ = a fixed constant -- a good approximation over a narrow frequency range not too close to any possible slot resonance frequency. In Case 2, we assume $x = h\phi$, where h is a design constant and ϕ is the electrical length of the transmission line between loading points. For TEM-mode propagation on the line, ϕ is linear with frequency, hence $x \propto \omega$ here. This is a viable assumption when the physical slot is narrow and not deep enough to produce a slot resonance near any frequency of interest. In a closed waveguide, ϕ will increase with increasing ω, though not linearly except when ω is well above the waveguide cutoff frequency. The overall phase shift per period is defined as θ. The analytical methods used are well known in circuit analysis and need not be detailed here.

Figure 16 is essentially a Brillouin diagram, except that the ordinate is ϕ rather than ω. Figure 16 applies to the case of Figure 15(a) with normalized x = constant = 0, 0.5, 1, 2, 4. With increasing x, narrowing of passbands and widening of stopbands is observed. Of course, the curves are not accurate for very small values of ϕ since the assumption X/Z_o = constant must break down in reality as $\omega \to 0$. For completeness, an upper passband for the system is shown ($\phi > 180^o$); its relevance is subject to the degree of validity of the assumption X/Z_o = constant over the frequency range involved.

Figure 17 plots Y/Y_o vs ϕ for the case at hand, and for the plane midway between loading elements. Whenever $Y/Y_o < 1$, the transverse impedance has been increased, as desired.

From Figure 17, it is seen that the transverse impedance approaches infinity as ϕ approaches the value for which cutoff ($\theta = 180^o$) occurs according to the chosen value of X/Z_o. Of course, the approach of the transverse impedance to infinity at low values of ϕ should be ignored; this is a consequence of the assumption X/Z_o = constant regardless of frequency. We note that in the upper passband ($180^o < \phi < 360^o$) the transverse impedance is <u>decreased</u>, in

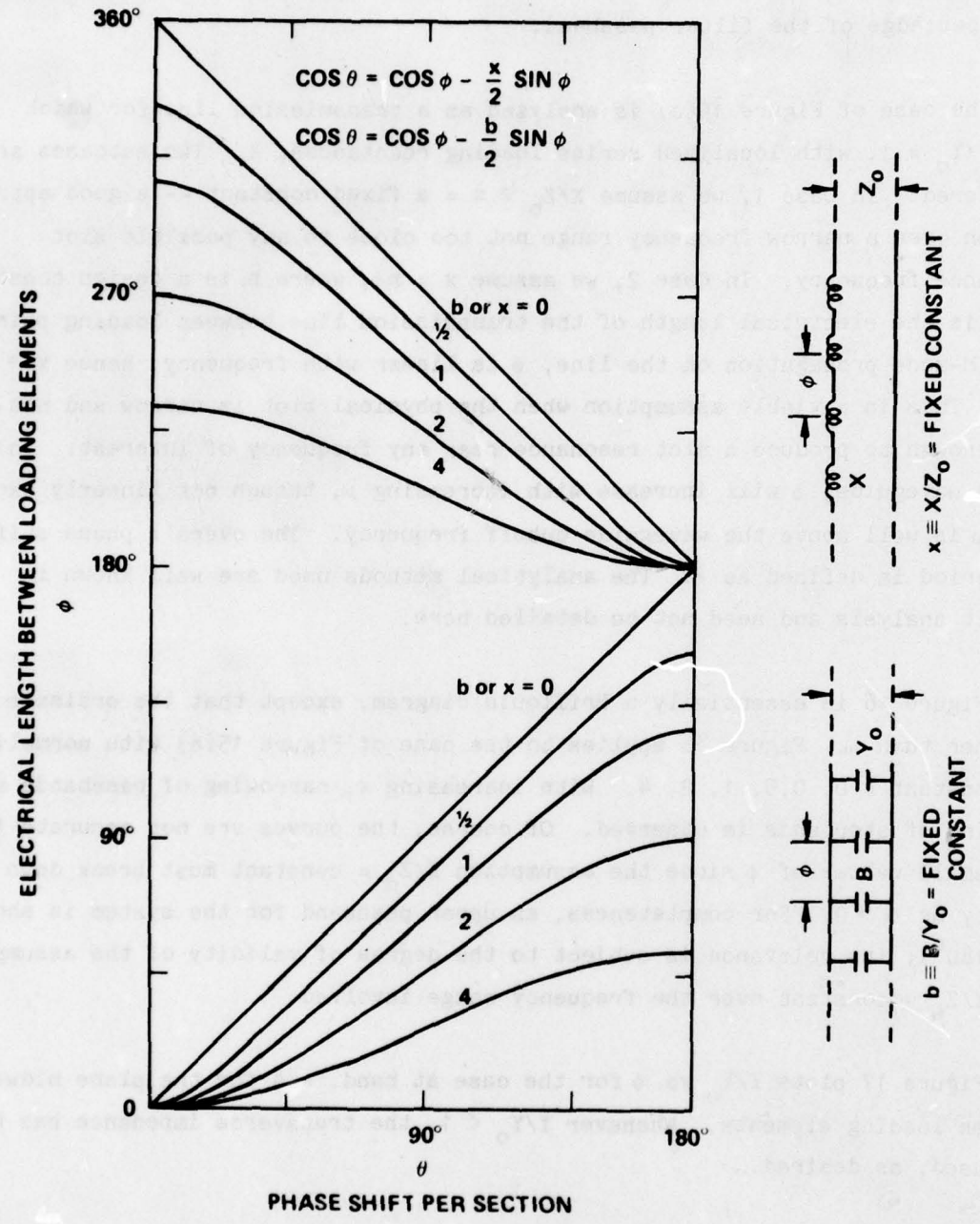

Figure 16. Brillouin-Type Diagram for Transmission Line with Periodic Loading by Either Lumped Series Inductances or Shunt Capacitances; Case 1, constant ratio of B to Y_o or X to Z_o.

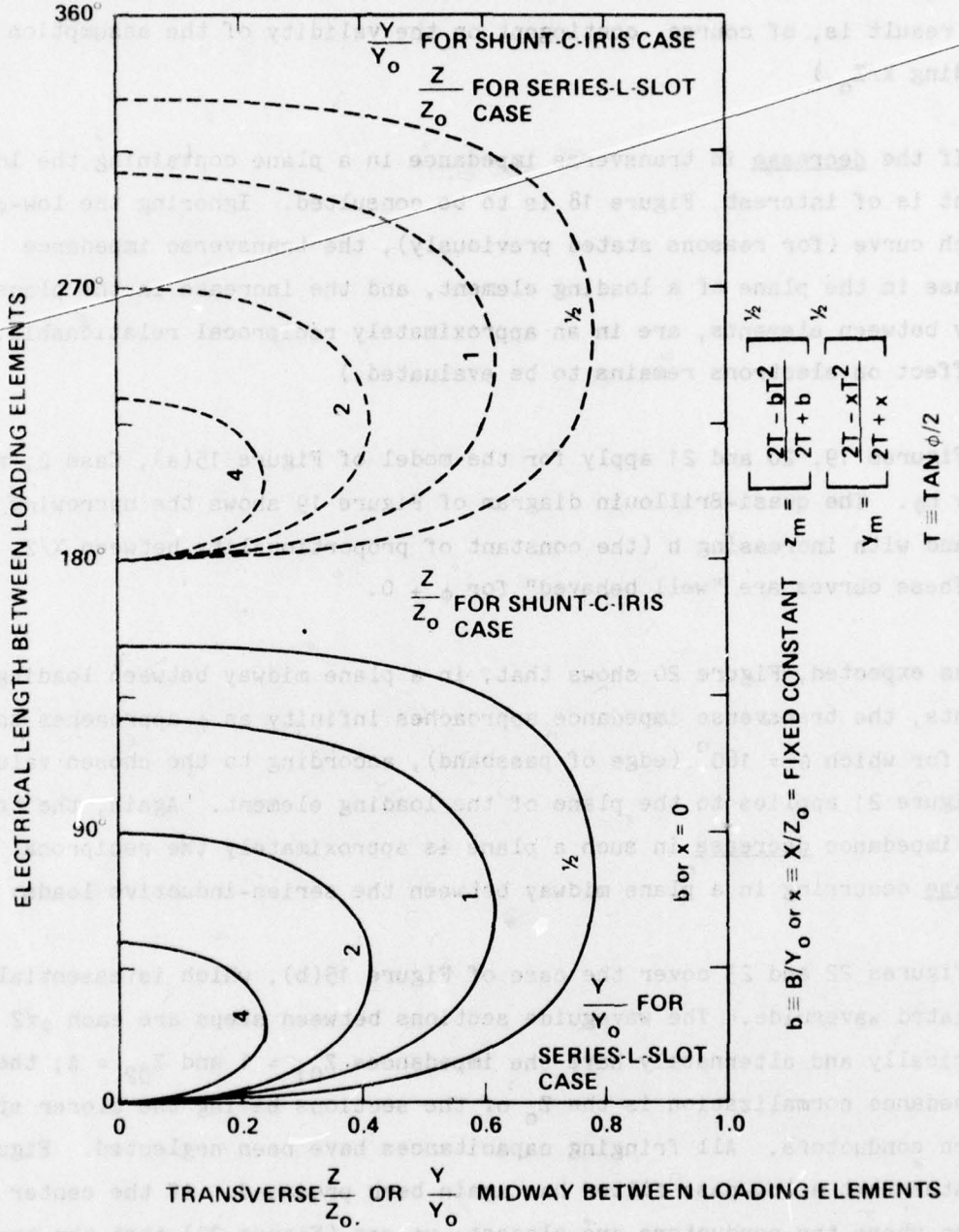

Figure 17. Normalized Transverse Impedance or Admittance Predictions for Case of Figure 16, Evaluated Midway Between Loading Elements

planes midway between loading elements, less the addition of such elements. (This result is, of course, contingent on the validity of the assumption regarding X/Z_o.)

If the decrease in transverse impedance in a plane containing the loading element is of interest, Figure 18 is to be consulted. Ignoring the low-ϕ tail of each curve (for reasons stated previously), the transverse impedance decrease in the plane of a loading element, and the increase in the plane midway between elements, are in an approximately reciprocal relationship. (The net effect on electrons remains to be evaluated.)

Figures 19, 20 and 21 apply for the model of Figure 15(a), Case 2, $x = X/Z_o = h\phi$. The quasi-Brillouin diagram of Figure 19 shows the narrowing of the passband with increasing h (the constant of proportionality between X/Z_o and ϕ). These curves are "well behaved" for $\phi \neq 0$.

As expected, Figure 20 shows that, in a plane midway between loading elements, the transverse impedance approaches infinity as ϕ approaches the value for which $\theta = 180^o$ (edge of passband), according to the chosen value of h. Figure 21 applies to the plane of the loading element. Again, the transverse impedance decrease in such a plane is approximately the reciprocal of the increase occurring in a plane midway between the series-inductive loads.

Figures 22 and 23 cover the case of Figure 15(b), which is essentially a corrugated waveguide. The waveguide sections between steps are each $\phi/2$ long electrically and alternately have the impedances $Z_{01} = 1$ and $Z_{02} = A$; the basis of impedance normalization is the Z_o of the sections having the closer spacing between conductors. All fringing capacitances have been neglected. Figure 22 indicates that a low-pass filter has again been produced. At the center of a section where the conductors are closest, we see (Figure 23) that the transverse impedance always exceeds the value prior to corrugating (Z_{01}) and approaches infinity at the upper edge of the passband. The more disparate the two waveguide heights (parameter A), the narrower the passband and the greater the enhancement of transverse impedance. However, at the center of a section where the conductors are furthest apart, the transverse impedance is decreased by an exactly reciprocal amount.

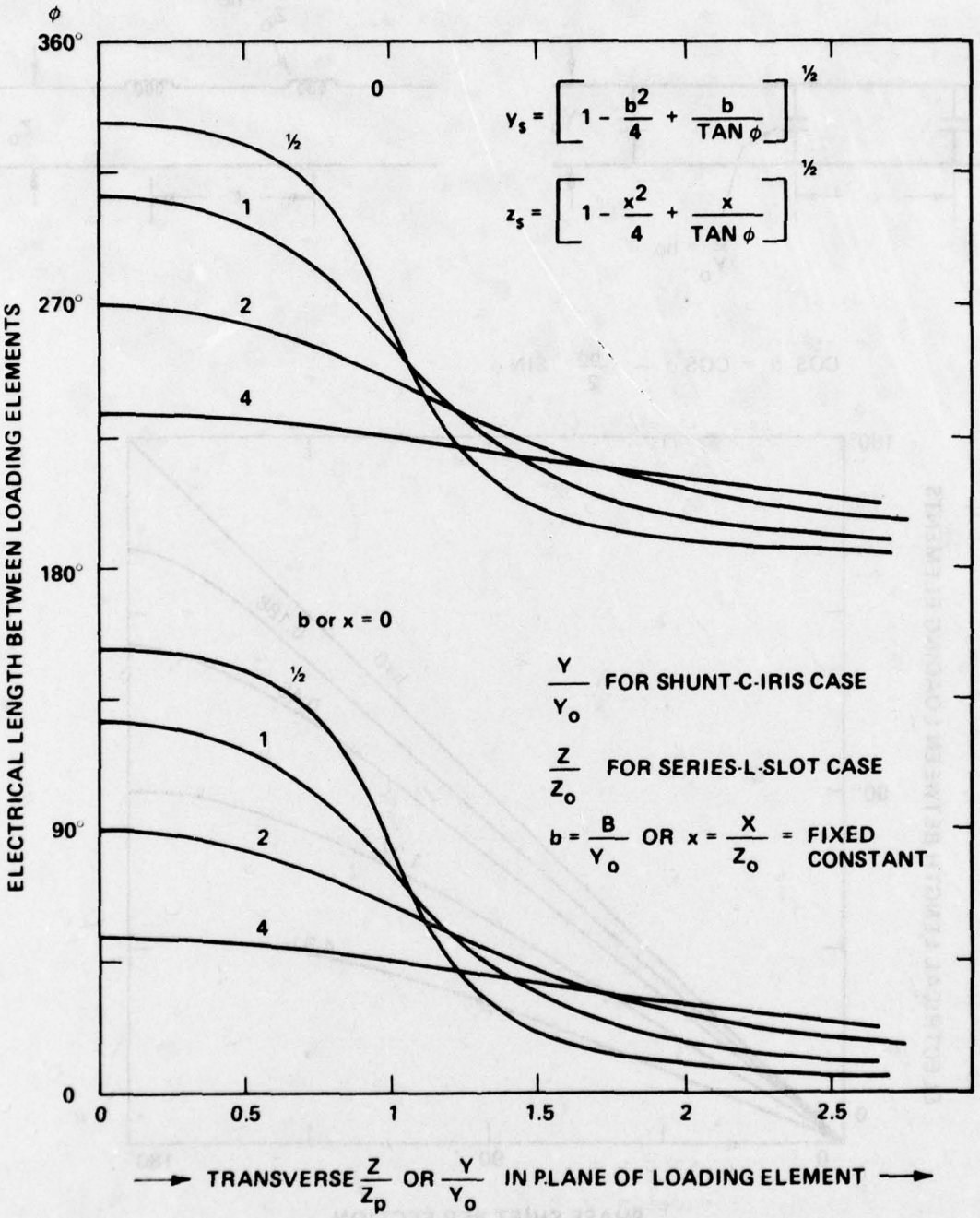

Figure 18. Normalized Transverse Impedance or Admittance Predictions for Case of Figure 16, Evaluated in Plane of Loading Element

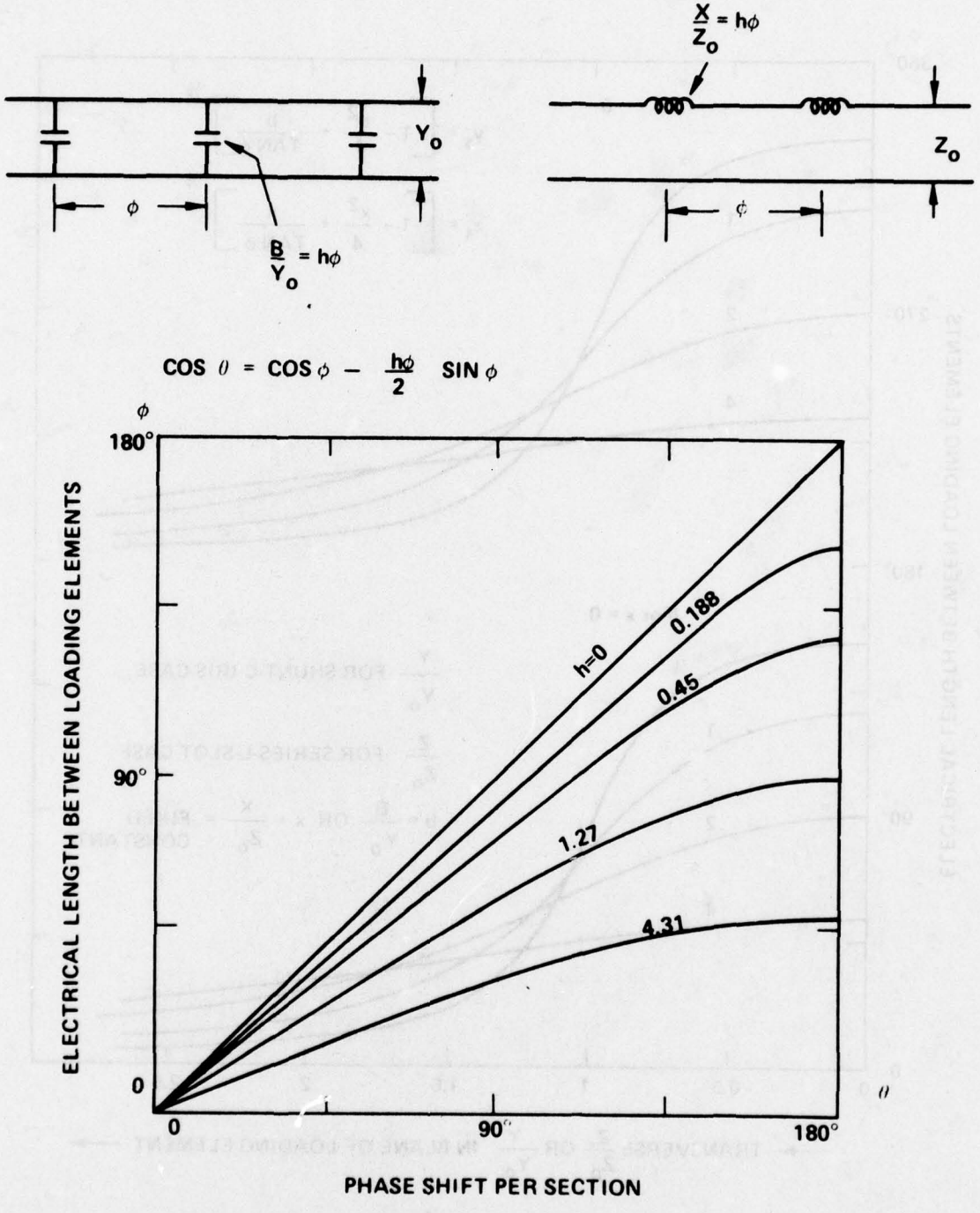

Figure 19. Brillouin-Type Diagram for Transmission Line with Periodic Loading by Either Lumped Series Inductances or Shunt Capacitances; Case 2, ratio B/Y_o or X/Z_o is Proportional to Electrical Length ϕ.

$$z_m \text{ or } y_m = \left[\frac{2T - h\phi T^2}{2T + h\phi} \right]^{1/2}$$

where $T = \tan \phi/2$

$$\frac{\beta}{Y_o} \text{ or } \frac{X}{Z_o} = h\phi$$

$\frac{Z}{Z_o}$ FOR SHUNT-C-IRIS CASE $\frac{Y}{Y_o}$ FOR SERIES-L-SLOT CASE

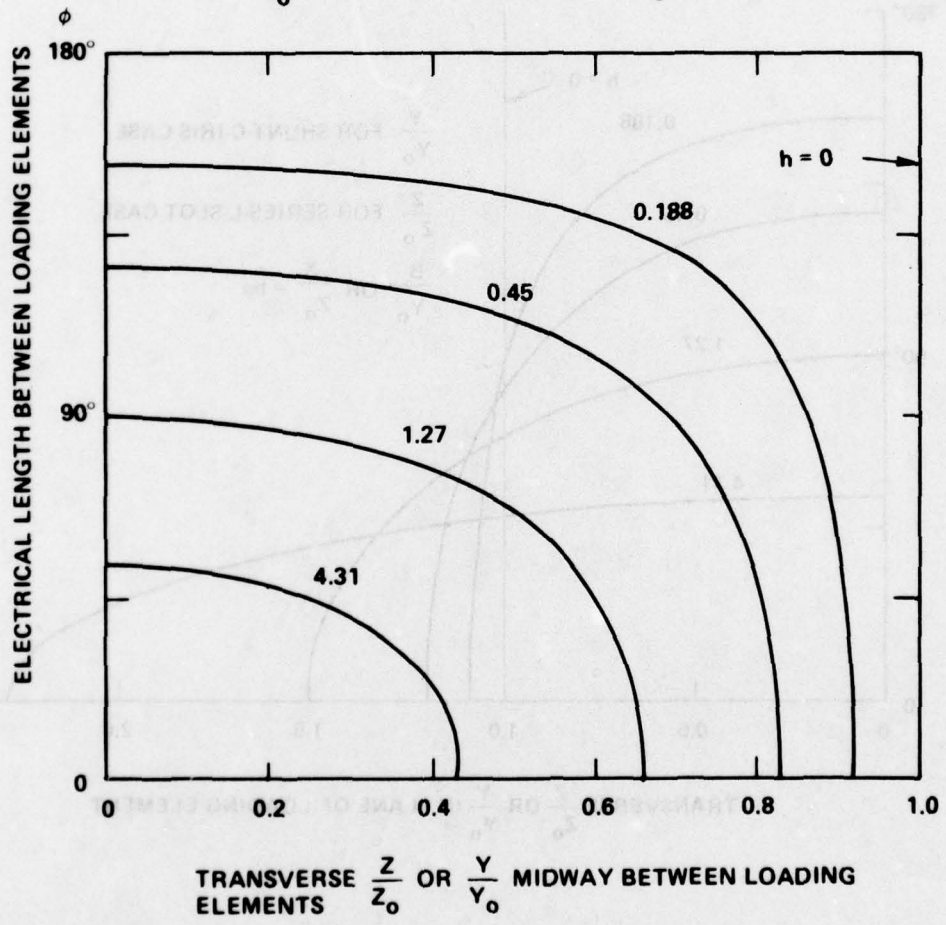

Figure 20. Normalized Transverse Impedance or Admittance Predictions for Case of Figure 19, Evaluated Midway Between Loading Elements

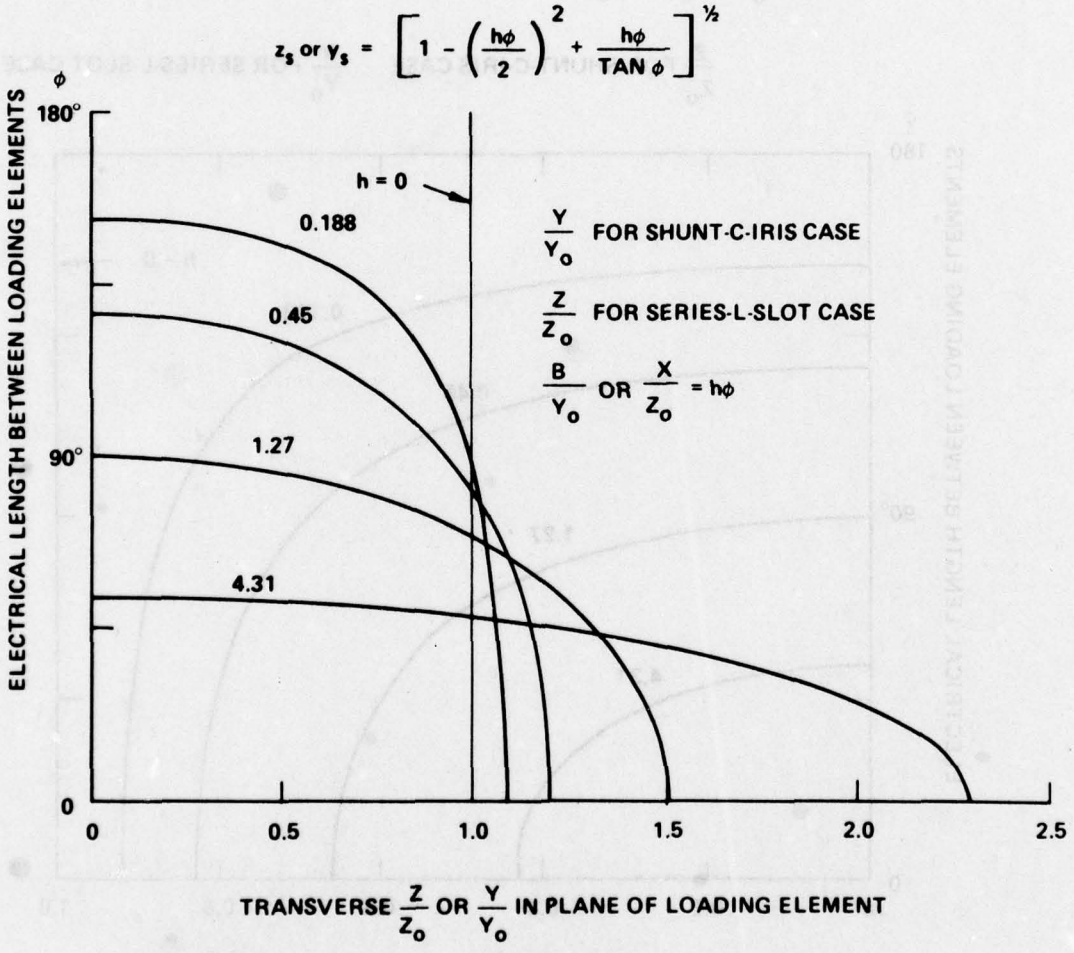

Figure 21. Normalized Transverse Impedance or Admittance Predictions for Case of Figure 19, Evaluated in Plane of Loading Element

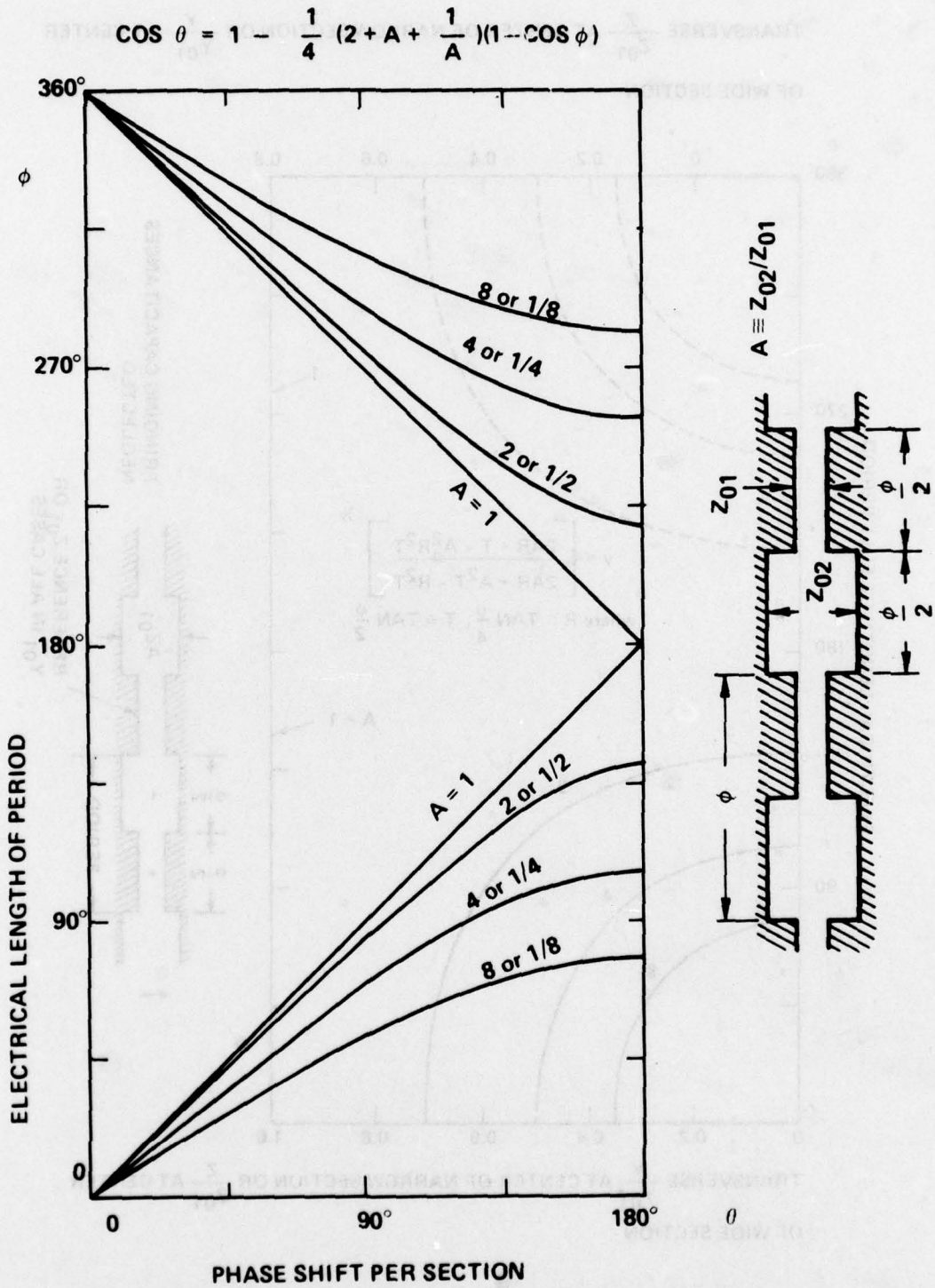

Figure 22. Brillouin-Type Diagram for Corrugated Transmission Line

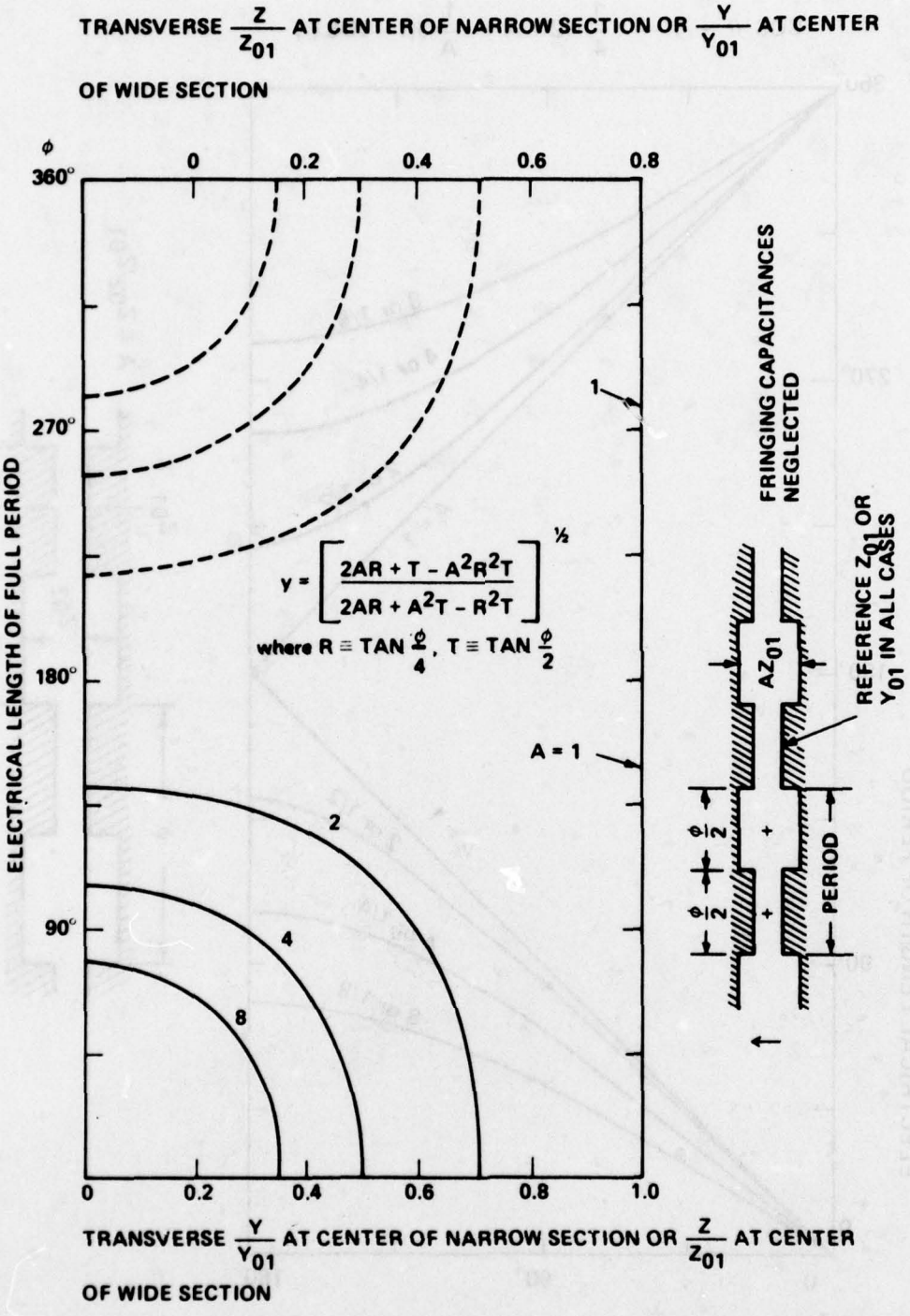

Figure 23. Normalized Transverse Impedance or Admittance Predictions for Case of Figure 22.

.or the case of Figure 15(c), the electrical behavior is describable by Figures 16 - 21, properly reinterpreted. Figure 15(c) gives a relatively wide-spaced transmission line (all impedances are now normalized to the Z_o corresponding to the widest spacing) periodically loaded with shunt-capacitive irises with $b \equiv B/Y_o$. Again we have Case 1, B/Y_o = a constant (Figures 16, 17, 18), or Case 2, $B/Y_o = h\phi$ (Figures 19, 20, 21). As expected, the transverse impedance tends to be increased in the plane of the capacitive iris and decreased, roughly reciprocally, in planes midway between irises. Of course, these values of transverse impedance are all relative to a Z_o that was high to begin with; this fact would be taken into account when predicting electronic interaction.

CONCLUSIONS

Although some simplifying assumptions have been made, we have generated models for estimating the trends of transverse-impedance change, and its variation with frequency, resulting from corrugating a transmission line, inserting localized series-inductive slots, or introducing localized shunt-capacitive irises. Basically, the transverse impedance rises in a plane where the conductors come closest together, and falls where the conductors move apart -- all relative to the Z_o of the unloaded transmission line. The overall effect on electrons gyrating and drifting through the line remains to be evaluated.

IMPLEMENTATION

We visualize a double-ridged rectangular waveguide, with the electron beam passing down the gap between the two ridges. The ridges will be serrated, according to Figure 15, (a) or (b) or (c), as appropriate. Since the lowest cutoff frequency can be very low here, we view this as a two-strip transmission line with periodic loading.

Alternatively, we can work with a simple TE_{10} rectangular waveguide. Series inductive stubs can be built onto the broad walls of the guide. Interestingly, it would suffice to simply cut transverse slots in the broad walls, or slots tilted at 45° in the narrow walls. Since the waves inside are slowed,

such slots will not radiate at frequencies below that for which the slot length is a half wavelength.

In a TE_{on} guide (circular electric), the cutting of rows of slots all over the pipe surface, with all slots fitted about 45^{o}, produces velocity slowing as is appropriate to the insertion of periodic series inductance. The phenomena here are well behaved (without radiation) at frequencies below that corresponding to a slot resonance.

IX. CONCLUSIONS AND PLANS

The gyro-TWT which has been built for the RADC-DARPA program appears to be giving relatively good agreement with small signal theory when one allows for the fact that the tube is relatively short and there is probably a very large loss associated with launching the growing, decaying and unattenuated waves of both TE_{11}^{o} mode polarizations.

So far results on most gyro-TWT experiments have been inconclusive. This may be due merely to lack of gain. It may, however, be due to more serious difficulties. We believe it is fortunate that we have a gyro-TWT which operates in the lowest waveguide mode and has a higher impedance circuit (two to three times higher value of E^2/P). If space-charge effects are an important limitation, our higher impedance circuit should give improved performance. Higher circuit impedance may also improve performance if velocity spread in the electron beam is a problem. We also believe, from the dispersion relations we have evaluated using high magnetic fields, that, in a gyro-TWT there may well be interaction at the operating frequency simultaneously in most or all of the waveguide modes with cutoff frequencies below the cyclotron frequency. This could lead to electron trajectories and bunches which are very strange indeed and would certainly lead to poor efficiency. Because our tube operates in the lowest waveguide mode we will not encounter this difficulty. For this reason, the further evaluation of our gyro-TWT approach is important.

Our biggest problem in completing this evaluation so far has been low gain due to the short length and high launching losses. However, we should now have increased the gain by putting an additional length of tubing in the body and installing the tube in a longer magnet which was available.

Once the saturation efficiency can be evaluated, we will be able to make interesting comparisons between our device and other gyro-TWTs such as those being studied at NRL. If the efficiency is only slightly greater than demonstrated in other experiments, it will be a good indication that the higher-impedance circuit gives more gain per unit length and hence is more

immune to space-charge problems. If this is the case, we should develop high-impedance circuits for gyro-TWTs. If, however, there is a very large change in the efficiency over other experiments, we believe it will indicate that the other experiments suffered from multimode bunching, and we should concentrate on lowest mode circuits.

In addition to completing the measurements on the existing tube and rebuilding it for higher gain, we anticipate that it will be necessary to build two more low frequency experimental tubes to arrive at the ideal circuit before we start the 94 GHz final design.

The following program schedule summarizes what we believe to be a sensible course of action in view of our present state of knowledge about gyro-TWTs.

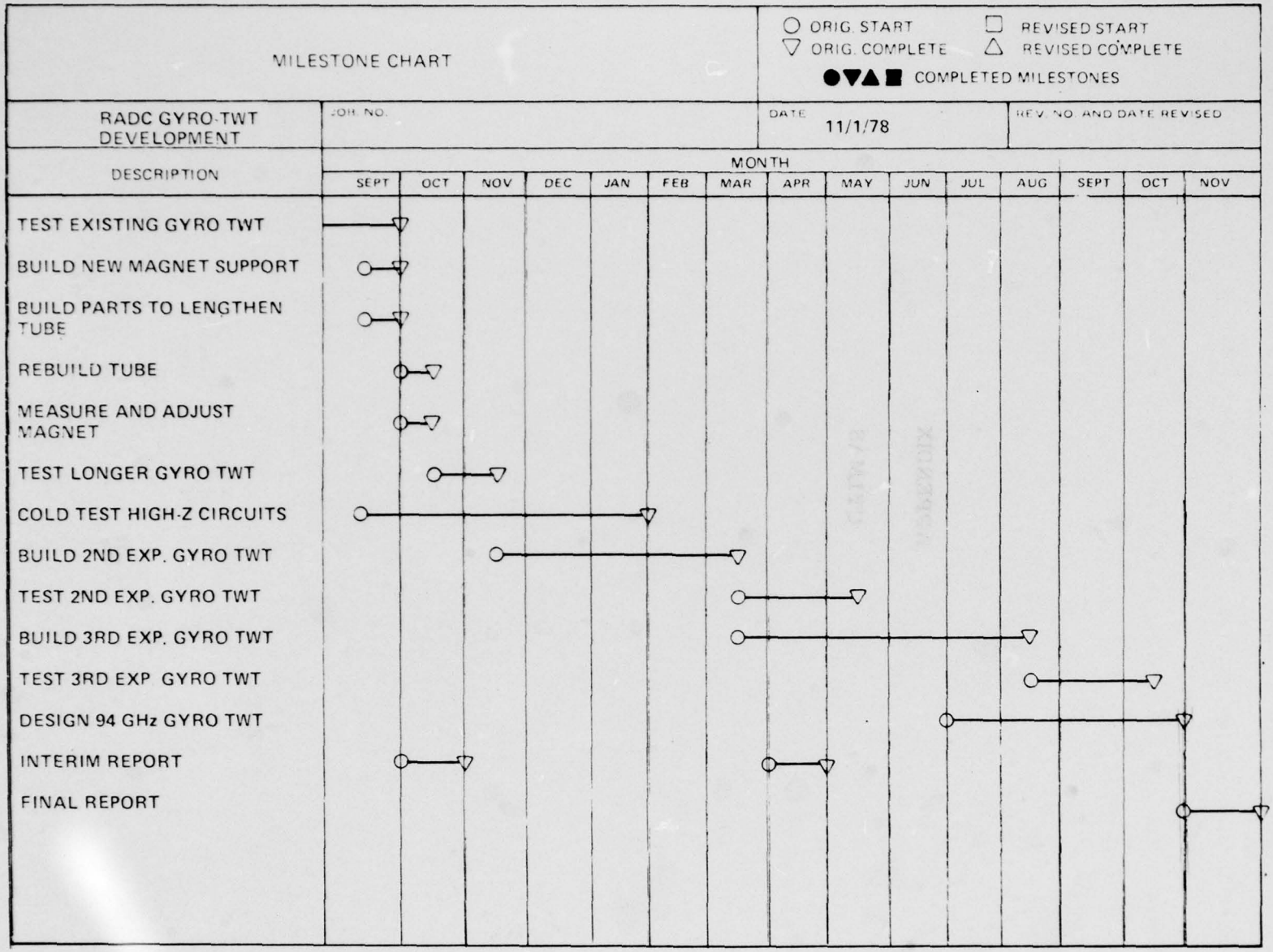
MILESTONE CHART
ORIG. START
REVISED START
ORIG. COMPLETE
REVISED COMPLETE
COMPLETED MILESTONES
RADC GYRO-TWT DEVELOPMENT
JOB NO.
DATE
11/1/78
REV. NO. AND DATE REVISED
DESCRIPTION
MONTH
SEPT
OCT
NOV
DEC
JAN
FEB
MAR
APR
MAY
JUN
JUL
AUG
SEPT
OCT
NOV
TEST EXISTING GYRO TWT
BUILD NEW MAGNET SUPPORT
BUILD PARTS TO LENGTHEN TUBE
REBUILD TUBE
MEASURE AND ADJUST MAGNET
TEST LONGER GYRO TWT
COLD TEST HIGH-Z CIRCUITS
BUILD 2ND EXP. GYRO TWT
TEST 2ND EXP. GYRO TWT
BUILD 3RD EXP. GYRO TWT
TEST 3RD EXP GYRO TWT
DESIGN 94 GHz GYRO TWT
INTERIM REPORT
FINAL REPORT

APPENDIX

CYLMAS

CYLMAS

A COMPUTER PROGRAM FOR CALCULATING OPTIMUM OPERATING PARAMETERS FOR A GYROTRON TRAVELING WAVE AMPLIFIER

Programmed by: A. T. Drobot
Naval Research Laboratory
Washington, D.C. 20375

Documentation: R. C. Morwood
Varian Associates, Inc.
611 Hansen Way
Palo Alto, California 94303

September 11, 1978

SUMMARY. The gyrotron is a new microwave tube dependent on the interaction between electrons in cyclotron orbits and the waveguide field inside a fast wave structure. The interaction between electrons following helical trajectories in an axial magnetic field and the waveguide fields originates in a relativistic effect.

Initial phases of the electrons are random. As electrons lose energy and become lighter, they rotate faster. Other electrons will gain energy and rotate more slowly. As electrons move through the waveguide, angular bunching takes place as a result of the angular velocity modulation. Bunching can be initiated at the beam entrance to the waveguide. As the beam travels down the tube and the bunching increases, energy interaction between the beam and the waveguide field can result in amplification gain.

The CYLMAS computer program was written at NRL[4] and has been modified to operate on the IBM 370/155 computer system at VARIAN. CYLMAS calculates gyrotron traveling wave amplifier performance, neglecting space charge, for cylindrical geometry and for the TE_{0n} waveguide modes.

This documentation is primarily a description of the computer program input and output with a minimum of theoretical discussion to aid in understanding what is required as program input and in interpreting program output.

PROGRAM INPUT. Input data is read into the program in NAMELIST format. For variables not present as input data, default values are assigned by the program. There are two NAMELIST names:

1. LSYST "Particle Namelist" contains most theoretical input data quantities

2. LRUNS "System Parameters Namelist" contains parameters affecting amount and form of output from the program, i.e., quantities to be printed and plotted.

Beam-wave interaction occurs around a frequency given by

$$\omega = s \Omega_b + k_z v_z$$

where ω is the wave frequency, k_z is the axial wave number, v_z is the axial electron velocity, s is the cyclotron harmonic number and Ω_b is the relativistic electron cyclotron frequency. Input quantities specify these parameters, plus information parameters relating to the waveguide mode number, and the numbers and positions of particles injected into the waveguide fields.

LSYST	Particle Namelist	Type of Variable	Default Value
NMOD	TE mode number, n, TE_{0n} mode, n = 1 to 10	Integer	1
NHRM	Cyclotron harmonic number = s	Integer	1
NEVR	Number of quantities per particle in beam frame. Presently V, Θ, and R. (Need not be specified unless program is changed to calculate additional quantities.)	Integer	4
MPGN	Number of values of γ the relative mass ratio	Integer	1
MPRR	Number of different radii rings can have	Integer	1
MPRN	Number of particles per ring	Integer	50

XFACT	Cyclotron frequency ratio = $x = \frac{\Omega_o}{\gamma_o \omega}$	Double Precision	1.0
NUFACT	Beam strength factor = Nu = N' r_e, where N' = total number of electrons per unit length and $r_e = \frac{e^2}{mc^2}$	Double Precision	0.002
GZERO	Average beam gamma $\left[\gamma_o^1 = 1 - \left(\frac{v_\perp}{c}\right)^2\right]^{-1/2}$ where, v_z = axial electron velocity at input and $v_\perp$ = perpendicular electron velocity at input	Double Precision	1.14
DELTG	Increment in gamma, $\Delta\gamma_o$	Double Precision	0.0
RZERO	Average beam radius = position of center of ring as a fraction of waveguide radius.	Double Precision	0.48
DELTR	Increment in ring radius (for additional ring positions)	Double Precision	0.0

There is a limitation on the total number of particles which may be launched and calculated by the program. NPAR = MPGN * MPRR * MPRN may not exceed 50.

LRUNS	System Parameters Namelist	Type of Variable	Default Value
	Control Variables of Run and Output Functions		
NSTOR	Store data every NSTOR cyclotron periods (Controls interval for printing and/or plotting "stored data" as specified by other parameters.)	Integer	1
MFAST	Number of time steps per cyclotron period	Integer	50
MSLOW	Number of cyclotron periods in the run	Integer	30
NVCEL	Number of cells in distribution functions	Integer	101
PNMAX	Maximum value on velocity distribution scale	Real	50.0

PNMIN	Minimum value on velocity distribution scale	Real	0.0
PVMAX	Maximum value of beta used in all plot diagnostics	Real	1.0
PVMIN	Minimum value of beta used in all plot diagnostics	Real	0.0

Control of Printed Output

LWPP	Print particle position, velocity and phase	Logical	.FALSE.
LWPI	Print particle betas during integration	Logical	.FALSE.
NWPP	Print betas for every JWPPth	Integer	1
IWPP	particle at every NWPPth slow	Integer	0
JWPP	cycle after the IWPPth slow cycle.	Integer	1
LWER	Print Error Diagnostics during slow cycles	Logical	.FALSE.
NWER	Print "orbit integration error"	Integer	1
IWER	for every JWERth particle at	Integer	0
JWER	every NWERth slow cycle after the IWERth slow cycle.	Integer	1
LWFR	Print values of field variables (E_θ and B_z).	Logical	.TRUE.
LWFi	Print values of field variables during integration.	Logical	.FALSE.
IWFR	Print field variables for	Integer	0
NWFR	every NWFRth slow cycle after the IWFRth slow cycle.	Integer	1

60

Control of Printer Plots

LPDI	Plot velocity distribution function.	Logical	.TRUE.
NPDI	Plot a velocity distribution for every NPDIth slow cycle after the IPDIth slow cycle.	Integer	1
IPDI		Integer	0
LPPH	Plot phase space β_θ vs β_r.	Logical	.TRUE.
NPPH	Plot phase space betas for every JPPHth particle very NPPHth slow cycle after the IPPHth slow cycle.	Integer	1
IPPH		Integer	0
JPPH		Integer	1
LPPL	Phase plots, β vs - λ(λ = space pitch angle)	Logical	.TRUE.
NPPL	Plot for every JPPLth particle and for every NPPLth slow cycle after the IPPLth slow cycle.	Integer	1
IPPL		Integer	0
JPPL		Integer	1

Control of CalComp Plots

LCRS	Plot stored data.	Logical	.FALSE.
LCPS	Plot stored particle data.	Logical	.FALSE.
LCAL	Determines if CalComp plots of any kind are to be done during the slow cycles.	Logical	.FALSE.

LCDI	Plot velocity distribution histograms.	Logical	.FALSE.
NCDI	Plot for every NCDIth slow cycle.	Integer	1
ICDI	Start plotting after ICDIth slow cycle.	Integer	0
LCPH	Plot β_θ vs β_r.	Logical	.FALSE.
NCPH	Plot for every NCPHth slow cycle.	Integer	1
ICPH	Start plotting after ICPHth slow cycle.	Integer	0
JCPH	Plot every JCPHth particle.	Integer	1
LCPL	Plot β vs $-\lambda$ if .TRUE.	Logical	.FALSE.
NCPL	Plot every NCPLth slow cycle.	Integer	1
ICPL	Start plotting after ICPLth slow cycle.	Integer	0
JCPL	Plot for every JCPLth particle.	Integer	1

Diagnostic Printing

LERR	Print "orbit integration error".	Logical	.FALSE.
LPRT	Print stored variables.	Logical	.TRUE.

Running Time Parameter

LAUT	(LAUT is not used in the VARIAN version of the program.)	Logical	.FALSE.

PROGRAM OUTPUT. Output from the CYLMAS program is in three forms: printed, printer plots, and CalComp plots. The order of printing, including plots on the printer, is:

1. Recapitulation of input data quantities and roots of the dispersion relation;

2. particle and field quantities at specified distances along the tube.

3. At the end of the calculation, both field and particle quantities are printed and plotted with respect to time.

CalComp plots are separate from the printer and the order of plotting is not important.

A number of error messages are possible and are printed any time the error is detected.

Printed program output is in the order described below.

Title. BEGIN CYLMAS RADIAL GEOMETRY V.1

Recapitulation of Input Quantities. The quantities in Namelist LSYST (see description of INPUT DATA) are printed before and after reading the Namelist.

IS = Harmonic number (NHRM in Input).
IN = Radial Mode Number (NMOD in Input).
NU = Beam strength parameter (NUFACT in Input).
GAMMAO = Initial beam energy (GZERO in Input).
X = Magnetic mistuning factor (XFACT in Input).
RHOO = Radial position as fraction of waveguide radius (RZERO).
VO = Average perpendicular velocity $v_\perp^2/c$
OMEGAE = Cyclotron frequency.

$$\text{RHOLO} = \frac{\sqrt{\gamma^2 - 1}}{\Omega_0}$$

HS = H in the dispersion relation
QS = Q in the dispersion relation
WE, WI, DELWR = roots of the dispersion relation.

The quantities in Namelist LRUNS (see description of INPUT DATA) are printed before and after reading the Namelist. Then, both Namelists are printed an additional time (as some quantities may have changed during the initial calculations.

Initial Conditions. CYLMAS 8.0 INITIAL CONDITIONS

X = Cyclotron frequency ratio
NU = Beam strength factor
GZERO = Average beam gamma (energy)
RZERO = Average beam radius
DELTR = Increment in Ring radii
CYCLOTRON FREQUENCY = OMEGAC
CUTOFF FREQUENCY = KN
TIME STEP DT
NMOD = The radial mode number
NHRM = The cyclotron harmonic
NPAR = The number of test particles
MFAST = Time steps per cyclotron period
MSLOW = Cyclotron periods in run

Diagnostics. During the integration of particles through the waveguide fields, and if indicated by the appropriate input parameter, the program will print and/or plot the following quantities at the end of each designated slow cycle.

1. Print "Particle Diagnostics", $\beta_\theta, \beta_r, \beta_\parallel, \beta_\perp$.

2. Print "Orbit Integration Error", $\beta_\theta, \beta_r, \beta_\parallel, \beta_\perp$.

PRECEDING PAGE NOT FILMED
BLANK

3. Print "Values of Field Variables", (E_θ and B_z fields).

4. Plot "Beta Distribution" Function.

5. Plot β_θ vs β_r phase space plot.

6. Plot β vs $-\lambda$ phase space plot, ($\beta_\perp$ vs atan ($\beta_\theta/\beta_\parallel$)).

Final Output. After integrating particles completely through the waveguide fields, i.e., after MSLOW slow cycles, the program prints and plots the following quantities in three tables.

I. STORED FREQUENCY DATA FROM E-THETA

TIME
ET FIELD = energy in E_θ field
GROWTH = growth rate of E_θ field, dB
SHIFT = phase shift of E_θ field

II. STORED FREQUENCY DATA FROM B-Z FIELD

TIME
BZ FIELD = energy in the B_z field
GROWTH = growth rate of B_z field, dB
SHIFT = phase shift of B_z field

III. STORED DIAGNOSTIC DATA

TIME
E-THETA = energy in E_θ field
B-Z FIELD = energy in B_z field
FIELD ENR = total field energy
KINETIC ENER = total kinetic energy
TOTAL ENER = field + kinetic energy
EFFICIENCY = $(\gamma - \gamma_o)/(\gamma - 1)$
AVERAGE R = average beam radius
BETA-PERP = $\beta_\perp$
BETA-THETA = β_θ
BETA-RADIAL = β_r
BETA-PARAL = $\beta_\parallel$
GAMMA = γ
1/GAMMA = $1/\gamma$

All quantities in all three tables are printed, then, if the proper input parameters are .TRUE. they will be plotted on the printer and/or the CalComp plotter.

Timing. After all calculations have been completed and all printing and plotting done, a final page will be printed showing the amount of cpu time required by the computer for each of twenty different phases of the computation.

1. Read data and calculate initial conditions, including solution of dispersion relation.
2. Print "Particle Diagnostics"
3. Print "Orbit Integration Error"
4. Print "Values of field Variables"
5. Plot "Beta Distribution" on printer
6. Plot "Beta-T vs Beta-R" on printer
7. Plot "Beta vs Lambda" on printer
8. Plot "Beta Distribution" on CalComp
9. Plot "Beta-T vs Beta-R" on CalComp
10. Plot "Beta vs Lambda" on CalComp
11. Integrate particles through fields and update field quantities
12. Calculate "Stored Quantities"
13. Print "Stored Quantities"
14. Plot "Stored Quantities" on printer
15. Not used
16. Plot "Stored Quantities" on CalComp

17.-20. Not used

Note 1. When an operation is repeated several times during a program run, the time is cumulative.

Note 2. In Item 16 above, only the cpu time required to prepare the data for plotting and transmittal to the plot tape is included. The actual CalComp plotting time is omitted.

A PARTIAL PROGRAMMERS' DOCUMENTATION

In addition to the MAIN program, the following subprograms are included in the CYLMAS program. Programs are listed according to segments of an overlay structure.

Root Segment (1)

MAIN
BES
BINBCD (VBPR)
CHAR (VBPR)
CLOCK (ALP)
LOGICAL$ (ALP)
PAVARG
PLOT$$ (VBPR)
PLOTL$$(VBPR)

Input Segment (2)

BJ
PDISPF
PDISPR
PES
PFILIN
PHSRS
PULLER

Computing Segment (3)

BOX
BPLOT
BROUND
DCPLOT
DPPLOT
DPRINT
ERRSQ
INTEG
PDIAGN
PFORCE
PORBIT
SUMSQ
ZERO
GETIME (VARIAN)
MAXVAL (VARIAN)

The MAIN program and all subprograms without parenthetic notes are substantially as obtained from NRL. Changes are restricted to those required to reduce array sizes and to introduce subprogram CALLS when necessary to accommodate Varian-written subprograms.

(ALP) designated subprograms were written at Varian in VM/370 Assembler Language for the IBM 370/155 computer.

The subprogram SUBROUTINE CLOCK returns the argument CPU time in minutes elapsed since beginning execution of the JOB.

The subprogram FUNCTION LOGICAL$ is a multi-entry function with entries:

LSHF - Logical shift, right or left
IAND - Logical AND
IOR - Logical OR

Subprograms designated (VBPR) are Varian Basic Plotting Routines. They are a set of machine-language routines which perform essentially the same functions as the CalComp plotting software.

Subprograms designated (VARIAN) are FORTRAN language subprograms written at Varian to perform the same functions as subprograms of the same names not received from NRL.

The subprogram FUNCTION GETIME (TIME) returns the CPU time in seconds since the beginning of the JOB. (GETIME, in turn, calls CLOCK).

The subprogram FUNCTION MAXVAL (X,NX) returns the index-1 of the member of the array, X, having the maximum value. ENTRY MINVAL returns the index-1 of the member having the minimum value. The size of the array, X, is NX.

..EFERENCES

1. Millimeter Wave Gyrotron Development, Phase I Final Technical Report. RADC-TR-77-210, June 1977. Contract F30602-76-C-0237, A041596.

2. High Power Millimeter Wave Amplifier Interim Report No. 1, Nov. 1, 1977 - Mar. 31, 1978, RADC Contract No. F306602-78-C-0011.

3. P. Sprangle and A. T. Drobot "The Linear and Self Consistent Nonlinear Theory of the Electron Cyclotron Maser Instability". IEEE Trans MTT, 25, No. 6, pp 528-544, June 1977.

4. K. R. Chu and A. T. Drobot "Theory and Single Wave Simulation of the Gyrotron Traveling Wave Amplifier Operating at Cyclotron Harmonics", NRL Memorandum Report 3788, Aug. 1978.